

1 Swilley, Tijerina-Kreuzer et al *Continental scale hydrostratigraphy: comparing geologically*
2 *informed data products to analytical solutions*

3

4 This manuscript has been submitted for publication in *Groundwater*. Please note that, despite
5 having undergone peer-review, the manuscript has yet to be formally accepted for publication.

6 Subsequent versions of this manuscript may have slightly different content. If accepted, the final
7 version of this manuscript will be available via the *Peer-reviewed Publication DOI* link on the
8 right-hand side of this webpage. Please feel free to contact any of the authors; we welcome
9 feedback.

10

11 **Continental scale hydrostratigraphy: comparing geologically informed data products to**
12 **analytical solutions**

13

14 Jackson S. Swilley (1), Danielle Tijerina-Kreuzer (1), Hoang V. Tran (2), Jun Zhang (3,4), Chen
15 Yang (1), Laura E. Condon (4), Reed M. Maxwell (1,5*)

16 (1) CEE, Princeton University; (2) Pacific Northwest National Laboratory; (3) Key Laboratory
17 of VGE of Ministry of Education, Nanjing Normal University; (4) HAS, University of Arizona;
18 (5) HMEI, Princeton University

19 *correspondence to: reedmaxwell@princeton.edu

20 **Abstract**

21 This study synthesizes two different methods for estimating hydraulic conductivity (K) at large
22 scales. We derive analytical approaches that estimate K and apply them to the contiguous US.
23 We then compare these analytical approaches to three-dimensional, national gridded K data
24 products and three transmissivity (T) data products developed from publicly available sources.
25 We evaluate these data products using multiple approaches: comparing their statistics
26 qualitatively and quantitatively and with hydrologic model simulations. Some of these datasets
27 were used as inputs for an integrated hydrologic model of the Upper Colorado River Basin and
28 the comparison of the results with observations was used to further evaluate the K data products.
29 Simulated average daily streamflow was compared to daily flow data from 10 USGS stream
30 gages in the domain, and annually averaged simulated groundwater depths are compared to
31 observations from nearly 2,000 monitoring wells. We find streamflow predictions from
32 analytically informed simulations to be similar in relative bias and Spearman's rho to the
33 geologically informed simulations. R-squared values for groundwater depth predictions are close

34 between the best performing analytically and geologically informed simulations at 0.68 and 0.70
35 respectively, with RMSE values under 10m. We also show that the analytical approach derived
36 by this study produces estimates of K that are similar in spatial distribution, standard deviation,
37 mean value, and modeling performance to geologically-informed estimates. The results of this
38 work are used to inform a follow-on study that tests additional data-driven approaches in
39 multiple basins within the contiguous US.

40

41 **Introduction**

42 While groundwater is the world’s largest accessible freshwater resource, it is intrinsically
43 difficult to characterize. Direct observations of groundwater can only be made using a limited
44 number of approaches, primarily monitoring wells, which are restrictive in scale. Remote sensing
45 has been used to create global-scale soil moisture products like Soil Moisture Active Passive
46 (SMAP) and Soil Moisture and Ocean Salinity mission (SMOS); however, these products are
47 most accurate up to 5 cm in depth and lend themselves better to land-surface applications than
48 groundwater availability applications (Jackson et al. 2012; Velpuri et al. 2015). Coarse estimates
49 of groundwater anomalies can be made using remote sensing products like GRACE (the Gravity
50 Recovery and Climate Experiment), but these estimates are made over large scales on the order
51 of $10^2 - 10^4 \text{ km}^2$ (Tapley et al. 2004; Scanlon et al. 2018). Management of this vital resource is
52 made even more challenging by the complex interrelation of groundwater with unsaturated zone
53 soil moisture, surface water, and even the lower atmosphere (Forrester and Maxwell, 2020;
54 Maxwell and Condon, 2016).

55 Hydrogeologic properties are similarly hard to observe. Hydraulic conductivity (K) is
56 typically inferred in groundwater models using a calibration or parameter estimation approach
57 (Hill and Tiedeman 2007). While common practice for more local to regional systems,
58 calibration approaches are still computationally impractical at large scales (Zell and Sanford
59 2020; Condon et al. 2021; Gleeson et al. 2021). Developing an accurate subsurface architecture
60 becomes even more important given the uncertainties and that alternate subsurface
61 representations are rarely explored (Enemark et al. 2019, 2020). Integrated hydrologic models
62 simulate surface and subsurface flow simultaneously. They can be used in a predictive sense and
63 to connect information from disparate observations like groundwater wells and stream gages. For

64 example, Foster et al. (2020) used numerical experiments to find that low-resolution models may
65 underpredict the effects of climate change on mountain headwater streamflows, and Forrester et
66 al. (2020) used scenario testing to determine how lateral groundwater flow affects
67 evapotranspiration in complex terrain. Continental-scale models are essential in many cases, as
68 some of the processes governing the hydrologic cycle, as well as many perturbations to the
69 hydrologic cycle, function at large scales (Eagleson 1986; Barthel 2014; Bierkens et al. 2015).

70 Physically based hydrologic models require the properties of the domain being simulated.
71 K is a critical input to any subsurface model (Freeze and Cherry 1979). This subsurface
72 parameter is important for accurate numerical modeling of groundwater systems and is a key
73 component of the analytical equations of groundwater flow as well. For modeling, an accurate 3-
74 D gridded representation of hydraulic conductivity is important for model performance (Turner,
75 1989). As mentioned above, calibration of hydraulic conductivity is a standard practice in
76 groundwater modeling, but computational demand makes the calibration of high-resolution,
77 continental-scale models to groundwater head or water table depths and streamflow
78 simultaneously, infeasible (Condon et al. 2021; Gleeson et al. 2021; O’Neill et al. 2021). A
79 common approach has been to assemble subsurface properties based on large scale datasets (e.g.,
80 de Graaf et al. 2020; Huscroft et al. 2018a), however newer approaches are evolving that are
81 semi-analytical (e.g., Luo et al. 2010a; Tashie et al. 2021) that provide an alternate pathway to
82 populating hydraulic conductivity values.

83 Our study develops and compares multiple continental-scale hydraulic conductivity
84 spatial models for the contiguous United States using two steps. The first step is a mapping
85 component in which several methods are used to estimate the saturated subsurface hydraulic
86 conductivity of the contiguous United States and adjacent hydrologic regions. These include

87 existing datasets, new combinations of existing data products and analytical solutions for
88 hydraulic conductivity calculated based on different assumptions. The second component of our
89 analysis is to evaluate how each hydraulic conductivity map influences the performance of an
90 integrated hydrologic model for an example test domain. We use selected 3D K fields as input to
91 a ParFlow-CLM integrated hydrologic model that simulates surface water and groundwater
92 simultaneously for a major US river basin, the Upper Colorado. Modeling results are compared
93 to observed streamflow and water table depths (WTD) for each subsurface data product. This
94 process assesses the performance of the hydraulic conductivity fields themselves and the
95 approaches used to develop them and their underlying assumptions.

96 **Understanding Hydraulic Conductivity**

97 The challenge of mapping hydraulic conductivity lies in the inability to observe it
98 completely. Unlike hydrologic features such as topography or stream density, hydraulic
99 conductivity cannot currently be observed or inferred using remote sensing techniques. Adding
100 to this challenge is the fact that hydraulic conductivity can vary by ten orders of magnitude or
101 more between differing subsurface media (Heath 1983), and the boundaries of these subsurface
102 media are difficult to map at high spatial resolution. Although K can be measured directly in a
103 lab using core samples or in situ using slug and pump tests, these methods are restrictive in scale
104 and can be expensive (Hornberger et al. 1998). Lab testing core samples measures the
105 conductivity of a single point in space at a very small support scale, meaning that the effects of
106 subsurface heterogeneity go largely unaccounted. While slug and pump tests directly measure
107 the effective hydraulic conductivity of real groundwater systems, their results are only
108 representative of the nearby subsurface on the order of meters to hundreds of meters (Hornberger
109 et al. 1998).

110 Hydraulic conductivity, when mapped at continental and global scales, is often assigned
111 by subsurface hydrogeology (Gleeson et al. 2014; Huscroft et al. 2018). This approach finds the
112 best available mapping of geology for a region and assigns a value of K for each geological unit.
113 We will refer to this type of approach as geologically informed throughout. The factor that
114 determines the accuracy of this approach is often data availability – in regions where geology is
115 mapped closely, K can be mapped similarly. One advantage of geologically informed approaches
116 is that they can be performed efficiently over large areas when the geology has been mapped and
117 it allows for local calibration and/or smaller-scale subdivision of these geologic units.

118 Analytical approaches to estimating K leverage assumptions on groundwater flow to
119 work backwards from observed hydrology to subsurface hydraulic properties. The advantage of
120 these approaches is that they may capture the effective hydraulic conductivity at the scale of
121 interest. This means that they would, ideally, capture the effect of features like faults, karst, and
122 fracture systems at scale, however this is untested in practice. Additionally, they do not suffer
123 from discontinuities at administrative boundaries, which are sometimes found in geology maps.

124 A methodology developed by Luo and colleagues is an analytical K estimation approach
125 that uses the geomorphology and hydrology of a domain (Luo et al. 2010b; Luo and Pederson
126 2012). We provide details on the application of this approach below but summarize briefly here.
127 Streams are assumed to be gaining, meaning that they receive baseflow from groundwater, and
128 the density of streams in a domain is assumed to negatively correlated to the permeability of that
129 domain (Luo et al. 2010b; Pederson 2001). This approach assumes that catchments are generally
130 in steady-state when considering the long-term averages of recharge and spring flows. Using this
131 assumption, a mass balance can be performed over a catchment, and hydraulic conductivity can
132 be estimated by making the DuPuit-Forchheimer assumptions and rearranging the groundwater

133 equation (Luo et al. 2010b). This approach, and similar approaches, represent promise as they
134 address the problem of effective K versus local K. They also represent efficient methods for
135 estimating hydraulic conductivity at large scales. To our knowledge, no study has evaluated the
136 results of such methods with an integrated hydrologic model.

137 In addition to relating hydraulic conductivity with stream density, our study also assumes
138 a relationship between topography and the water table of unconfined aquifer units. The
139 relationship between topography and the water table of unconfined aquifers has been recognized
140 since the 19th century (King 1899). It is commonly said in hydrology that the water table
141 behaves as a “subdued replica of the ground surface,” and we will use this principal to equate
142 large-scale averages in topographic slope to average hydraulic gradient (Desbarats et al. 2002).
143 There remains, however, some question over how and when this relationship can be used.
144 Desbarats et al. (2002) explains the advantages and challenges of relating topography and
145 groundwater elevation in application when producing two models to map groundwater depth
146 using a digital elevation model. Haitjema and Mitchell-Bruker (2005) discuss the circumstances
147 under which water tables are topography controlled and conversely recharge controlled, but
148 ultimately conclude that there is nearly always some degree of correlation at large scales.

149 We will use Luo’s approach as an example of an analytical approach from literature and
150 Huscroft’s GLHYMPS 2.0 data product as an example of a geological K mapping from
151 literature. It is important, however, to acknowledge approaches that we do not consider in our
152 analysis. There are many continental and global-scale K products that make use of pedotransfer
153 functions to estimate hydraulic properties of soil from more easily measurable properties; (Gupta
154 et al. 2021; Jarvis et al. 2013; Montzka et al. 2017; Rahmati et al. 2018) to name a few. These
155 approaches could be considered a subcategory of geologically informed approaches. We choose

156 not to include a pedotransfer approach or product because their focus is on shallower soil units,
157 and ours is up to 1.2 km of subsurface hydrostratigraphy. We have also not included the Tashie
158 et al. (2021) analytically informed K data products who use hydrograph recession analysis to
159 estimate the watershed-scale effective hydraulic conductivity of the contiguous US, or the
160 shallow calibrated transmissivities of Zell and Sanford (2020), both of which were not available
161 when this work was being undertaken and are for shallower systems than we consider in this
162 work.

163

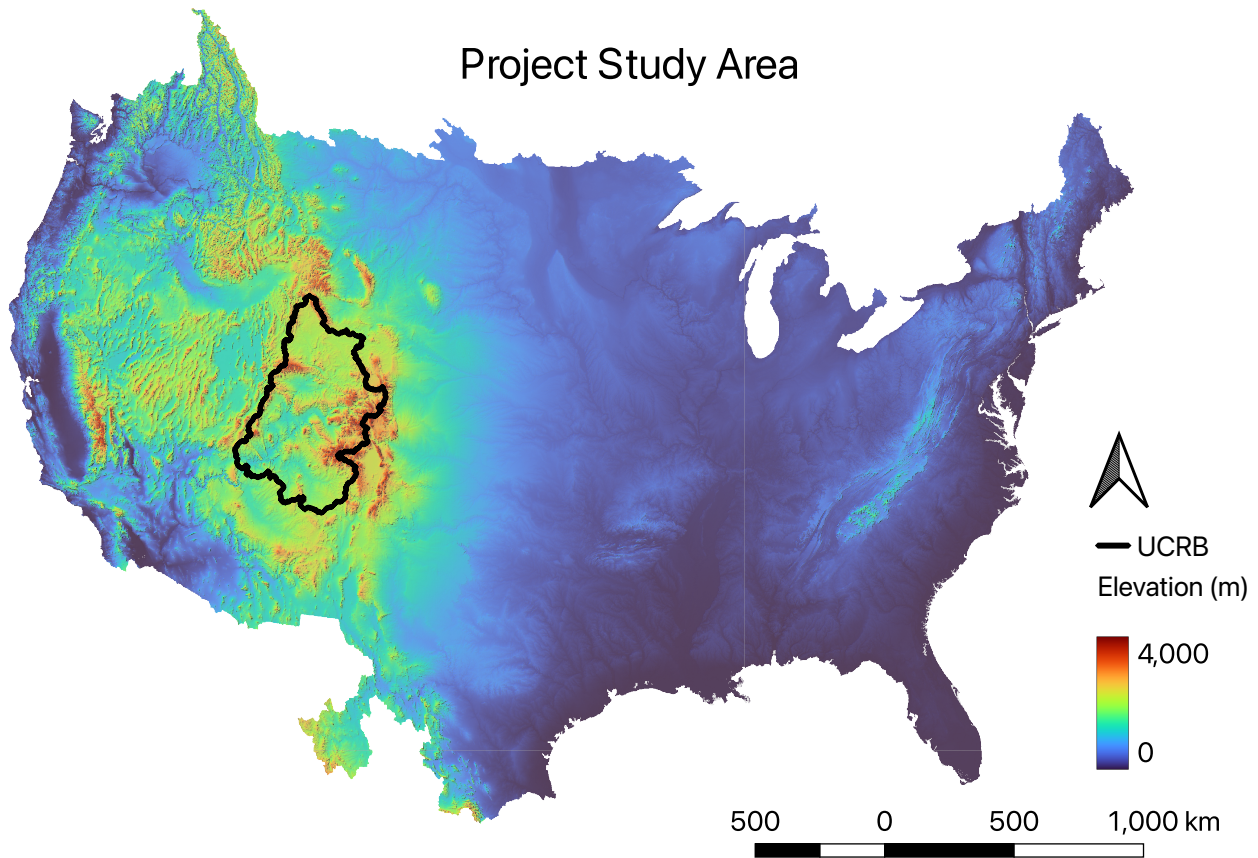
164 **Methods**

165 Our process for this study begins with using several methods to map saturated subsurface
166 hydraulic conductivity for the contiguous United States. We categorize these approaches as
167 *geological*, meaning that K is assigned based on knowledge of the subsurface geology and
168 *analytical*, meaning that they rely on a mathematical formulation. We create six hydraulic
169 conductivity maps using an analytical approach from literature; we create six more maps using
170 an analytical approach derived in this study, and we compare with three geologically-derived
171 maps; two of which were compiled or edited for this study, and a third which was taken directly
172 from literature. These two-dimensional products are then combined into a 3D K field. We
173 discuss and evaluate the statistics of the K fields derived from these different approaches.

174 These three-dimensional K fields are then used as subsurface inputs to the integrated
175 hydrological model, ParFlow-CLM of the Upper Colorado River Basin (UCRB) to evaluate how
176 each mapping influences model performance. ParFlow-CLM simulates surface water and
177 groundwater simultaneously and is driven by hourly atmospheric forcing for an entire water year.
178 Simulated daily streamflows are compared to daily flow data from 10 USGS stream gages in the
179 domain, and annually averaged simulated groundwater depths are compared to observations from
180 nearly 2,000 monitoring wells. We would like to emphasize here that this test basin is intended
181 only to illustrate the ways that different K data products can influence model behavior. This is
182 not intended to be an exhaustive national modelling study.

183 We perform all mapping analyses over the contiguous US and areas outside the US
184 connected to major US river basins. Figure 1 provides an outline of the full study area with the
185 UCRB modeling subdomain delineated in black. This spatial extent was chosen to include all
186 areas that drain to US, such as the Columbia River Basin and the full Rio Grande Basin, for

187 future modeling efforts. Mapping is done in 2D at high resolution with grid cells of one square
188 kilometer. Analytical approaches average hydrologic parameters of a catchment at the US
189 Geological Survey (USGS) Hydrologic Unit Code, HUC12 scale; HUC12s are watershed areas
190 mapped by the USGS on the order 10^2 km² on average. Geologically informed K maps, those
191 with vector geometry originally, are rasterized at the aforementioned one-kilometer resolution as
192 are the borders of the HUC12 catchments. Table 1 provides a full list of the hydraulic
193 conductivity products considered in this study.



194
195 Figure 1. Hydraulic conductivity mapping domain with modeling subdomain: the contiguous
196 United States and inward-flowing watersheds and the Upper Colorado River Basin (UCRB).
197

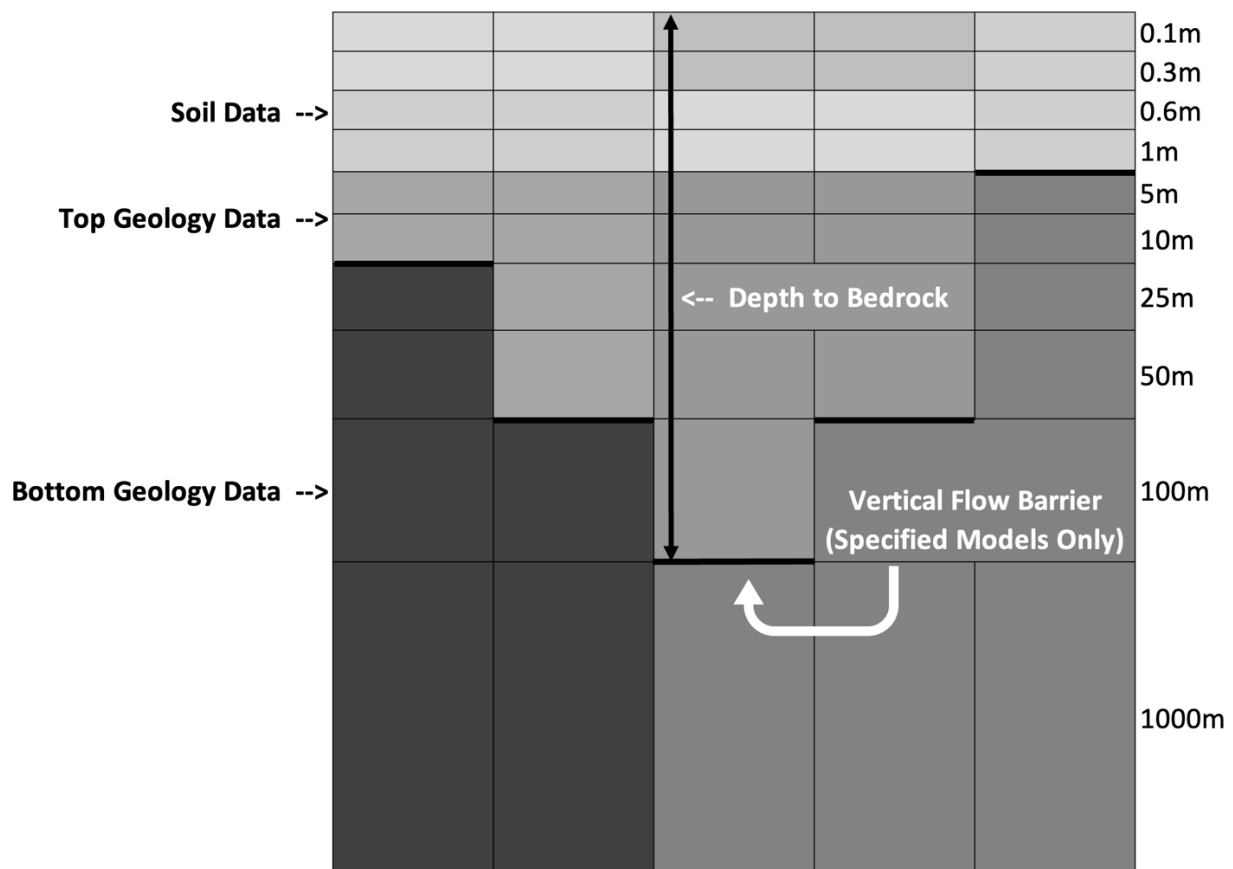
198 *Geological Methods*

199 The geologically informed maps use existing datasets to assign K values (Figure 3, Table 1). The
200 first of the geologically informed data products is the GLHYMPS 2.0 dataset from Huscroft et al.
201 (2018b), referred to from here forward as *Geological K Case 1*. This product is composed of two
202 vertical layers, with the top layer extending from the surface to an estimated depth of bedrock
203 provided by Shangguan et al. (2017) and the second layer beneath. The upper layer
204 predominantly represents unconsolidated areas, while the lower layer predominantly represents
205 the underlying geology (Huscroft et al. 2018b). It is important to note that these layers are
206 properties of the dataset itself, independent of model layers. When applying the dataset to our
207 modeling application, we assign properties of the top layer to cells with centers above
208 Shangguan’s estimate of depth to bedrock and properties of the bottom layer to cells with centers
209 beneath it. A depiction of this vertical disaggregation can be seen in Figure 2.

210 The second geologically informed data product is created by assigning K values from
211 Heath (1983) to a geology map created by the USGS (Belitz et al. 2019). This K field will be
212 referred to as *Geological K Case 2* mapping hereinafter. The USGS geology map used is the
213 union of the USGS Principal Aquifer dataset and Secondary Hydrogeologic Regions dataset
214 (Belitz et al. 2019). Combined, these two maps cover the entirety of the US. Outside of US
215 borders, *Geological K Case 1* geology values are used.

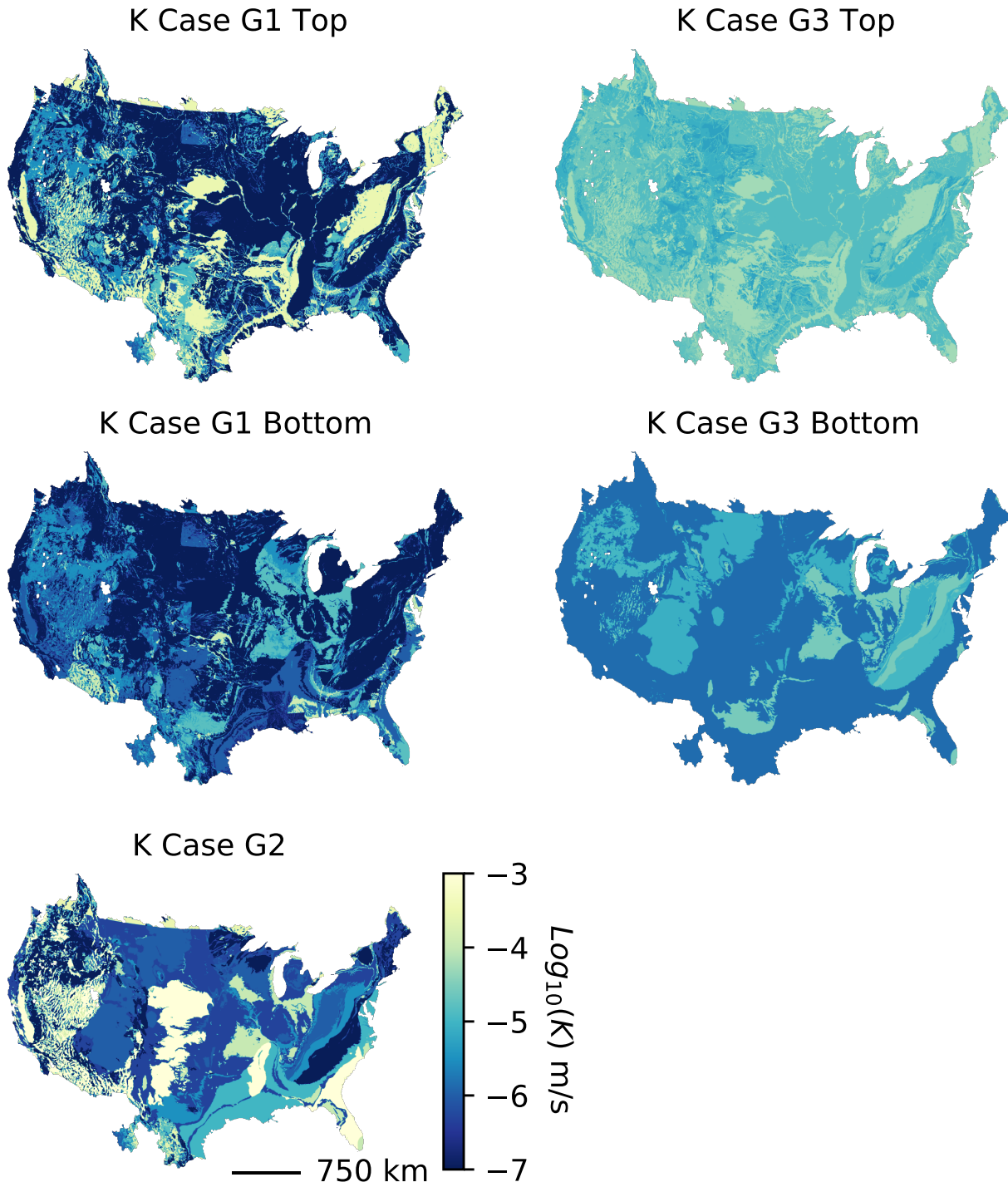
216 Our study considers a third geology-informed data product for comparison. This K field
217 uses the geometries from *Geological K Cases 1* and *2* but assigns estimates of K from Maxwell
218 et al. (2015) to each rock type. Described in detail in Maxwell et al. (2015), these values are a
219 combination of the Gleeson et al. (2011) values and other literature values. This is a two-layer
220 product – the upper layer is the top layer of the *Geological K Case 1* map, and the bottom layer

221 is the *Geological K Case 2* geometry. As in *Geological K Case 1*, the top layer is mapped down
222 to the Shanguan estimated depth of bedrock. The idea supporting this approach is that the top
223 layer of *Geological K Case 1* focuses on the unconsolidated, near-surface units, and *Geological*
224 *K Case 2* focuses on deeper units. Unconsolidated areas are mapped as bedrock in the lower
225 layer below the depth to bedrock product. This is done because the underlying dataset is
226 vertically-averaged, and unconsolidated areas are expected to be accounted for by *Geological K*
227 *Case 1* in the upper layer. We will refer to this product as *Geological K Case 3*. All K fields are
228 summarized in Table 1.
229



230
231 Figure 2. Conceptual model of 3D hydraulic conductivity and vertical discretization of test
232 domain (not drawn to scale). Note that certain features identified here may change depending on

233 the case simulated such as the presence of the flow barrier as described in Table 3, or the discrete
234 nature of K values for the *Geological* cases.



235

236 Figure 3. Geologically informed hydraulic conductivity data products. See Table 1 for
237 definitions.

238 *Analytical Methods*

239 As mentioned previously, we use two analytical approaches in this study. Using these two
 240 analytical approaches with different assumptions, we create and assess a total of 12 mappings—
 241 9 for actual hydraulic conductivity (L/T) and 3 for transmissivity (L/T^2)—based on the
 242 combination of analytical approach and assumptions (Table 1) and input data (Figures S1-S6).

243 The first analytical approach that we implement was developed by Luo et al. 2010. From
 244 here forward, this approach will be referred to as the *Literature Analytical Approach*. This
 245 method starts with the conceptual diagram shown in Figure 4, develops an equation for steady-
 246 state flux to the stream and inverts for hydraulic conductivity. Luo et al. (2010, 2012) derive this
 247 equation for flux based on the Dupuit equation. We briefly rederive the Luo et al. (2010)
 248 formulation here starting from Darcy’s law combined with a simple statement of continuity. If
 249 we start with the Darcy equation:

$$250 \quad q' = -Kb \left(\frac{\Delta h}{\Delta x} \right) \quad (1)$$

251 Where K is the effective hydraulic conductivity [L/T], h is the hydraulic head [L], x is a distance
 252 along the hillslope, b is the average aquifer thickness expressed as $b = \frac{(H-(H-d))}{2}$, and q' is the
 253 flux from *both* hillslopes that drain into the stream as shown. If we assume no underflow (or
 254 inter-basin flow) from neighboring hillslopes, we can say that $q' = 2RW$ where R is the effective
 255 recharge [L/T], W is the length from hilltop to stream [L] and the factor of two appears because
 256 q' represents the flow from both hillslopes shown in Figure 4. H is the aquifer thickness [L],
 257 assumed to be from the bedrock to the top of the hillslope and d is the valley depth [L], or the
 258 change in elevation or topography from the top of the hillslope to the stream.

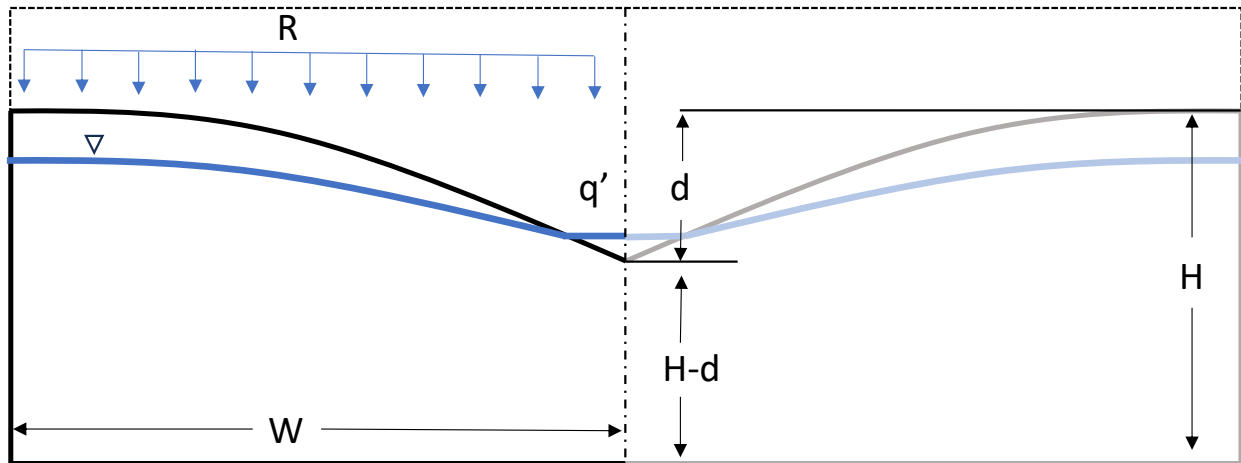
259 The change in head in (1) may be written as $\Delta h = (h - d) - H$ [L] and the distance
 260 becomes $\Delta x = W$ [L]. If we combine and simplify we get:

261
$$2RW = \frac{K}{2W} (H^2 - (H - d)^2) \quad (2)$$

262 When we solve (2) for K we get:

263
$$K = \frac{4RW^2}{(H^2 - (H - d)^2)} \quad (3)$$

264 Which is the same as EQ (2) in Luo et al. (2012). Note that this same solution is obtained using
 265 the Dupuit derivation and setting the constants of integration based on the system as shown in
 266 Figure 4. This analytical solution assumes that catchments are effectively drained, aquifer
 267 thickness is equal to depth-to-bedrock, and groundwater flow is horizontal. As the length from
 268 hilltop to stream is not always easily determined, the drainage density [L^{-1}] may be used in place
 269 of W .



270
 271 Figure 4. Conceptual model of hydrologic catchment properties modified after (Luo et al.
 272 2010b).

273 Drainage density (D), while not depicted in Figure 4, is roughly equivalent to $1/2W$,
 274 where W is the average flow length to the nearest stream for water that falls in a catchment (Luo
 275 et al. 2010b). D can be estimated by dividing the total length of streams in a catchment by the
 276 catchment's area. W can be calculated by averaging the downstream distance from every location
 277 in a watershed to the nearest stream. If drainage density is used then Equation (3) becomes:

278
$$K = \frac{R}{D^2[H^2-(H-d)^2]} \quad (4)$$

279 Both terms, D and W , will be tested by our analytical K cases. These parameters are
280 derived using the National Hydrography Dataset (NHD) Plus stream map (U.S. Geological
281 Survey 2019). Parameters such as: recharge, aquifer thickness, valley depth, and drainage
282 density, are averaged over each USGS HUC12 catchment (U.S. Geological Survey 2019). These
283 parameters are used in Equation 4 to estimate K for each catchment and are illustrated in Figure
284 4.

285 Hydraulic gradient is assumed to be a function of aquifer thickness and valley depth,
286 which is defined as the average depth of erosion along streams. Valley depth can be
287 approximated by taking the black top hat transform of a digital elevation model (Rodriguez et al.
288 2002). This study performs the black top hat transform at ~30m resolution over the entire
289 contiguous US, as shown in the supporting information, Figure S5. The resulting black top hat
290 transform is then averaged at 250m resolution for storage and use. To convert this 250m black
291 top hat product to valley depth, it is then averaged along the NHD streams for each catchment.

292 Aquifer thickness is assumed to be equivalent to the depth of bedrock. This means that
293 the *Literature Analytical Approach* assumes that unconsolidated areas are fully saturated some
294 distance away from their draining streams and that bedrock geologies do not contribute to
295 baseflow. Further assumptions on the value of aquifer thickness and valley depth are necessary
296 as well in this approach. The mathematical formula of the *Literature Analytical Approach*
297 produces negative hydraulic conductivities when valley depth is more than twice aquifer
298 thickness. We test three assumptions that remedy this problem: 1) assuming aquifer thickness is
299 greater than or equal to 100m. 2) assuming valley depth is less than or equal to aquifer thickness.
300 3) assuming aquifer thickness is a constant 200m. These assumptions are outlined in Table 1.

301 Finally, recharge was estimated by subtracting average evapotranspiration from precipitation
 302 (Tran et al. 2020). These two parameters were averaged over each catchment for calculation.

303 The second analytical approach, which is first proposed in the current study, is a variation
 304 of the Luo’s method where the hydraulic gradient is assumed to be equivalent to topographic
 305 slope (Zhang et al. 2021). This new formulation alleviates the need for the additional
 306 assumptions on aquifer thickness and valley depth. This study’s approach is used for the creation
 307 of both hydraulic conductivity sets and transmissivity (T) sets. The formulas for these methods
 308 are provided below by Equations 5 and 6. For two cases, one K and one T, slopes and flow
 309 lengths from the UCRB ParFlow model were used instead of the true landscape slopes and flow
 310 lengths to assess the importance of inner consistency when modeling permeabilities.

311
$$K = -\frac{RW}{SH} \quad (5)$$

312
$$T = -\frac{RW}{S} \quad (6)$$

313 K – hydraulic conductivity (L/T)

314 T – transmissivity (L²/T)

315 R – average recharge (L/T)

316 W – effective flow length (L)

317 H – aquifer thickness (L)

318 S – topographic slope (L/L)

319

320 Table 1. Summary and description of subsurface data products and the resulting K fields.

Name	Layers	Method	Assumptions
------	--------	--------	-------------

Geological K Case 1 (K Case G1)	2	K values from Huscroft (2018); Shangguan depth to bedrock (2016)	NA
Geological K Case 2 (K Case G2)	1	USGS Primary Aquifers and Secondary Hydrologic Regions assigned K values by this study	NA
Geological K Case 3 (K Case G3)	2	GLYMPS 2.0 geometry over USGS Primary Aquifer geometry assigned K by this study; Shangguan depth to bedrock (2016)	ParFlow Indicators
Analytical K Case 1 (K Case A1)	1	Literature analytical method (Luo et al 2010) with drainage density and aquifer depth (H) larger than 100m	$H \geq 100$ m
Analytical K Case 2 (K Case A2)	1	Literature analytical method (Luo et al 2010) with drainage density and valley depth (d) limited to aquifer depth	$d \leq H$
Analytical K Case 3 (K Case A3)	1	Literature analytical method (Luo et al 2010) with drainage density and aquifer depth (H) set to a constant value	$H = 200$ m
Analytical K Case 4 (K Case A4)	1	Literature analytical method (Luo et al 2010) with average effective flow length (same as Case A1 above but with effective flow length)	$H \geq 100$ m

Analytical K Case 5 (K Case A5)	1	Literature analytical method (Luo et al 2010) with average effective flow length (same as case A2 but with effective flow length)	$d \leq H$
Analytical K Case 6 (K Case A6)	1	Literature analytical method (Luo et al 2010) with average effective flow length (same as case A3 but with effective flow length)	$H = 200 \text{ m}$
Analytical K Case 7 (K Case A7)	1	This study’s analytical method using average effective flow length	NA
Analytical K Case 8 (K Case A8)	1	This study’s analytical method using drainage density	NA
Analytical K Case 9 (K Case A9)	1	This study’s analytical method using average effective flow length	Model slopes and flow lengths
Analytical T Case 1 (T Case A1)	1	This study’s analytical method using average effective flow length	NA
Analytical T Case 2 (T Case A2)	1	This study’s analytical using drainage density	NA
Analytical T Case 3 (T Case A3)	1	This study’s analytical method using average effective flow length	Model slopes and flow lengths

321 In some areas of our domain, we did not have sufficient data for one or more of the
322 required input parameters. Gaps in the input data hampered the application of the analytical
323 solutions in these regions, primarily in HUC12s with limited NHD Plus stream data. To address
324 this, we implement two data filling techniques. No-data areas inside of US borders are filled
325 using simple nearest neighbor interpolation for smoothness. No-data areas outside of the US

326 borders, which are larger on average, are extrapolated using a linear ridge model from Scikit
 327 Learn (Pedregosa et al. 2011). For both hydraulic conductivity and transmissivity, the
 328 extrapolation model is trained on recharge and elevation, as our analytical solutions are sensitive
 329 to both of these parameters. Table 2 in the supporting information shows the percentages of the
 330 domain interpolated and extrapolated for each analytical case.

331

332 Table 2. Percentages of domain interpolated and extrapolated.

K Field	Interpolation %	Extrapolation %	Total %
Analytical K Case 1	15.79	5.72	21.51
Analytical K Case 2	16.18	5.72	21.90
Analytical K Case 3	15.77	5.72	21.49
Analytical K Case 4	15.88	5.72	21.60
Analytical K Case 5	17.00	5.72	22.72
Analytical K Case 6	15.83	5.72	21.55
Analytical K Case 7	2.63	5.72	8.35
Analytical K Case 8	15.78	5.72	21.50
Analytical K Case 9	3.06	5.72	8.78

333

334 *Modeling Methods*

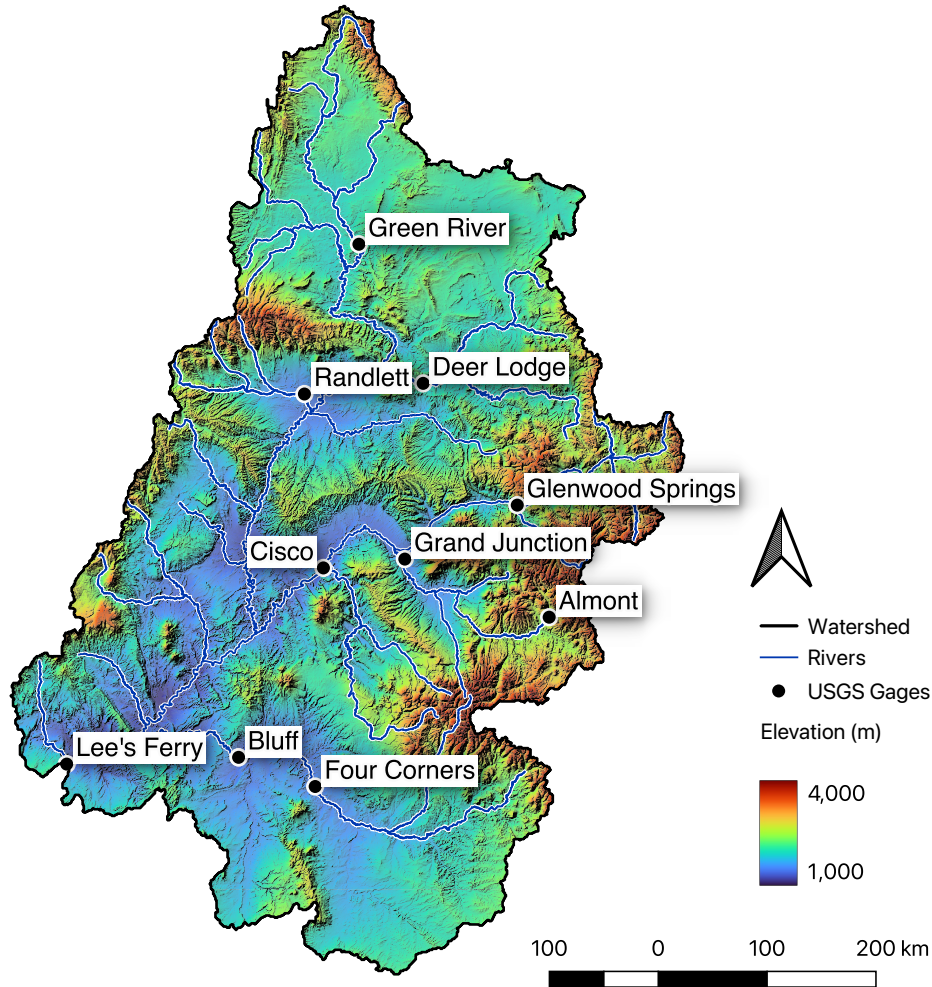
335 The UCRB is approximately 284,898 km² in area and covers portions of Wyoming, Colorado,
 336 Utah, New Mexico, and Arizona (Figure 1). It encompasses high-elevation mountain headwaters,
 337 lower prairie land and even deserts, making it hydrologically diverse. The UCRB is also

338 topographically constrained and large in extent, meaning that the lateral flow through the edges
339 of the domain are much smaller than other subbasins. The UCRB also has a range of topography
340 and a mix of rain and snow processes across its extent. Despite the water management present in
341 this system (which was not considered in the simulations) we still felt this was an optimal choice
342 as a test domain. Modeling is performed for the water year of 1983 in the UCRB. The water year
343 chosen and UCRB domain are advantageous as there is clear seasonality in flow regimes due to
344 snow melt allowing baseflow and peak flows to be analyzed separately. We use this opportunity
345 to disentangle the surface water controls of subsurface hydraulic conductivity (e.g., Foster and
346 Maxwell, 2019). The dramatic snowmelt-driven peak flows of 1983 also allow us to observe
347 model performance in extreme conditions.

348 The model used for simulations is ParFlow-CLM, a 3D integrated hydrologic model,
349 coupled to the land surface model, CLM (Ashby and Falgout, 1996; Jones and Woodward, 2001;
350 Kollet and Maxwell, 2006, 2008; Maxwell, 2013; Maxwell and Miller, 2005). The UCRB is
351 modeled at 1km horizontal resolution and varying vertical resolution; the vertical discretization
352 can be seen in Figure 2. CLM, a land surface model, is used in all simulations, and hourly
353 NLDAS meteorological forcing for the water-year of 1983 drives meteorological inputs (Xia et
354 al. 2014). Eight meteorological variables (wind, two component solar, pressure, temperature,
355 precipitation, humidity) were bilinearly interpolated to each grid cell to create this forcing dataset
356 which was then used to drive the CLM portion of ParFlow-CLM. Each simulation case was
357 spun up using a two-step approach, first a steady state P-ET forcing product followed by two
358 years of transient simulation. Soil data from STATSGO2 makes up the first 2m of each model
359 domain, with our hydraulic conductivity fields beneath (Figure 2) (Soil Survey Staff n.d.). An
360 additional advantage of Geological K Case 3 is that the soil layers have spatially variable

361 porosities and van Genuchten water retention properties. These properties are associated with the
362 geologic indicators in ParFlow-CLM used in this test case, documented by Condon and Maxwell
363 (Condon and Maxwell, 2014; Condon and Maxwell, 2013).

364 Modeled stream flows are compared to observed flows from USGS stream gages at 10
365 locations in the UCRB (Figure 5). We take an unweighted arithmetic mean of streamflow at
366 USGS gage points so that headwaters have suitable representation. Simulated water table depth
367 (WTD) is compared to observation well data (Fan et al. 2013). In this comparison, WTD is
368 calculated as a free water table below the ground surface, averaged over the water year, which is
369 consistent with the Fan et al (2013) database.



370

371 Figure 5. Model domain: Upper Colorado River Basin above Lee's Ferry.

372

373

374

375

376

377

378

We ran a total of 10 simulations beginning with one K case from each analytical approach and our three geological K maps for comparison. After concluding the first five simulations, we moved forward with an additional five simulations; this time making use of a model element referred to as a vertical flow barrier, which simulates confining units by reducing flow at specified model cell interfaces (Marshall et al. 2022). The depth at which the vertical flow barrier is applied can be constant or can vary laterally (see Figure 2). We apply the flow barrier to reduce, but not eliminate, vertical flow between simulated deeper groundwater systems

379 and the unconfined upper units that typically interact more dynamically with surface water. For
 380 four analytical cases, we apply the vertical flow barrier at the depth that was used to define the
 381 aquifer thickness when calculating K thus reducing the transmissivity of the simulated
 382 unconfined upper aquifer to the same as was implied by the approach. We also ran a simulation
 383 using the *Geological K Case 1* product combined with a vertical flow barrier at Shangguan’s
 384 estimate of depth to bedrock for comparison. Table 3 provides a full list of the modeling
 385 simulations run and the method of assigning a vertical flow barrier.

386 Table 3. Modeling simulations. Note: CFBZ indicates a constant-depth flow barrier and SFBZ
 387 indicates a variable-depth flow barrier at Shangguan’s depth to bedrock. The modified variable-
 388 depth flow barrier (mSFBZ) is located at a depth of 100m or Shangguan’s estimate of depth to
 389 bedrock, whichever is greater.

Subsurface	Vertical Flow Barrier Depth
Geological K Case 1	Vertical flow barrier not used
Geological K Case 2	Vertical flow barrier not used
Geological K Case 3	Vertical flow barrier not used
Analytical K Case 1	Vertical flow barrier not used
Analytical K Case 7	Vertical flow barrier not used
Geological K Case 1	Variable-depth flow barrier: SFBZ
Analytical K Case 1	(modified) Variable-depth flow barrier: mSFBZ
Analytical K Case 7	Variable-depth flow barrier: SFBZ

Analytical K Case 3

Constant, 192m-depth flow barrier:

CFBZ

Analytical T case 1

Constant, 192m-depth flow barrier:

CFBZ

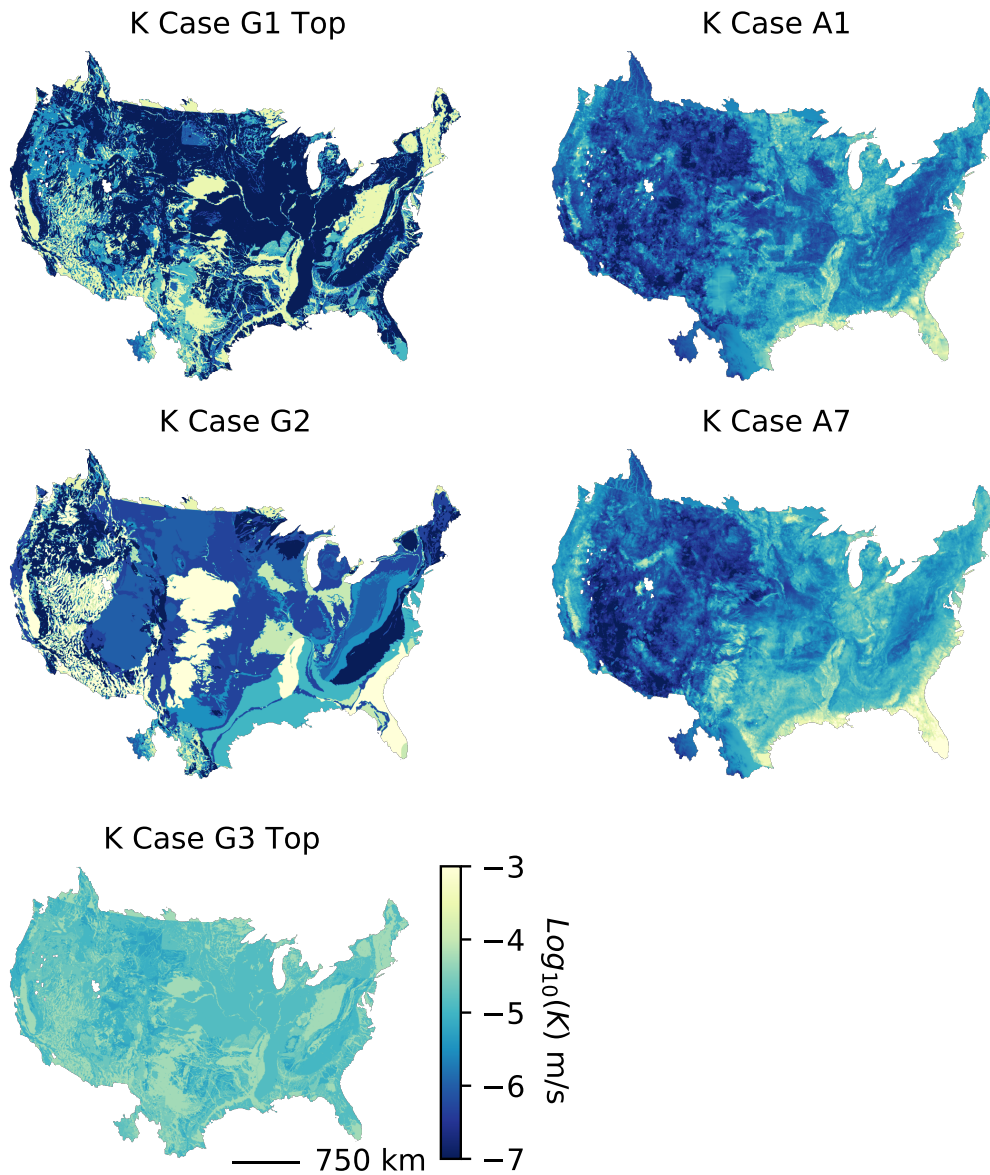
391 **Results**

392 *Hydraulic Conductivity Data Product Results*

393 We evaluate six hydraulic conductivity data products using the *Literature Analytical Approach*,
394 and three hydraulic conductivity solutions and three transmissivity solutions for the using *this*
395 *study's analytical approach*. The spatial distribution of K in five representative hydraulic
396 conductivity products can be seen in Figure 6. We see the two analytical approaches produce K
397 maps that are very similar in value and spatial distribution. When comparing geological K maps
398 with analytical maps, a few features are present in all. This includes the Mississippi Embayment
399 and California's Central Valley; the High Plains aquifer is also faintly visible. Areas that
400 disagree between analytical and geological K maps include the Midwest and Basin and Range.
401 Our large-scale mean conductivities resemble those of geology-informed approaches from
402 literature as seen in Table 4. Figures S7 and S8 in the supporting information present all nine
403 hydraulic conductivity maps and all three transmissivity maps from analytical approaches.

404 We find that K values derived from analytical approaches are slightly higher on average
405 with smaller standard deviations than K values derived from geologically informed approaches
406 (Table 4, Figure 7). The exception to this finding is *Geological K Case G3*, which has a higher
407 mean and smaller standard deviation than the analytically derived K fields. Analytical cases 2
408 and 5 trend towards the highest Ks among the *Literature Analytical Approach* cases. Both of
409 these cases assume that valley depth d was less than or equal to aquifer thickness H . This result
410 highlights the sensitivity of the *Literature Analytical Approach* to the relationship of valley depth
411 with aquifer thickness. *Analytical K Case 9* and *Analytical T Case 3* appear to be outliers among
412 the *Study Analytical Approach results*. This is due to the fact that model slopes, which are
413 calculated at a resolution of 1000m, the resolution of the hydrologic model, instead of 250m,

414 were used to infer hydraulic gradient, thus decreasing slope and increasing K values. Table 4
415 offers a statistical comparison of all K products and Figure 7 presents the probability density
416 functions of each analytically derived set and the probability mass function of each geologically
417 informed product.

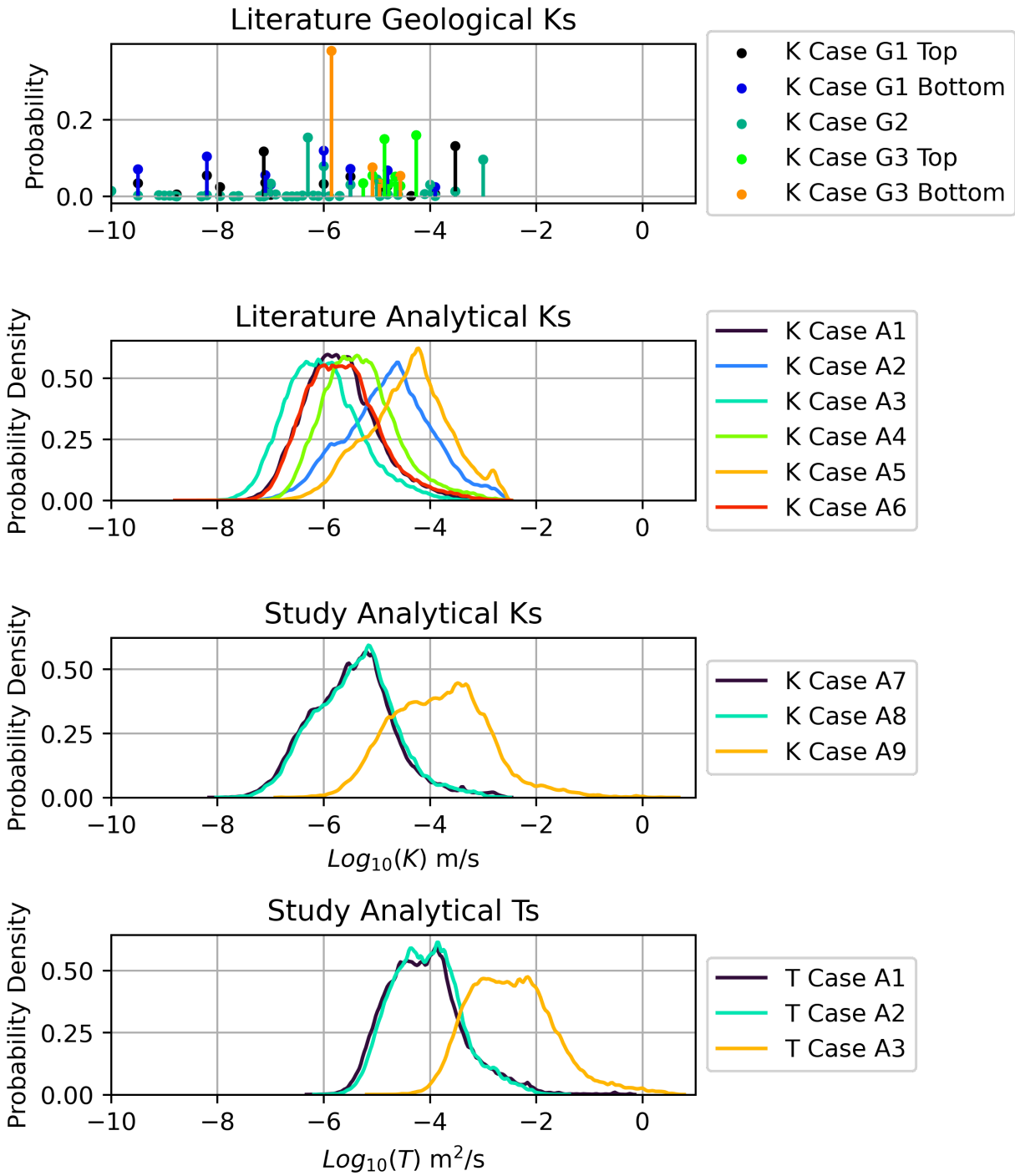


418
419 Figure 6. Comparison of analytically and geologically derived hydraulic conductivity data
420 products. White inland areas in all products represent lakes without any estimated value of K.

421 Table 4. Statistical comparison of analytically and geologically derived hydraulic conductivity
 422 values. Conductivities in in m/s, transmissivities in m²/s.

Name	Log-Transformed Data		Untransformed Data	
	Mean	STD	Mean	STD
Geological K Case 1 (top layer)	-5.79	1.90	9.83E-05	1.39E-04
Geological K Case 1 (bottom layer)	-6.77	1.54	6.40E-06	2.19E-05
Geological K Case 2	-5.37	1.69	1.80E-04	3.28E-04
Geological K Case 3 (top layer)	-4.64	0.33	2.99E-05	2.02E-05
Geological K Case 3 (bottom layer)	-4.88	0.23	1.53E-05	8.81E-06
Analytical K Case 1	-5.68	0.69	9.65E-06	3.72E-05
Analytical K Case 2	-4.77	0.82	8.83E-05	2.44E-04
Analytical K Case 3	-6.01	0.70	5.09E-06	2.90E-05
Analytical K Case 4	-5.31	0.70	2.71E-05	1.13E-04
Analytical K Case 5	-4.41	0.77	1.57E-04	3.38E-04
Analytical K Case 6	-5.63	0.72	1.46E-05	7.09E-05
Analytical K Case 7	-5.45	0.79	2.77E-05	1.38E-04
Analytical K Case 8	-5.41	0.76	2.16E-05	8.80E-05
Analytical K Case 9	-3.80	0.92	3.58E-03	4.53E-02
Analytical T Case 1	-4.10	0.72	1.00E-03	1.43E-02
Analytical T Case 2	-4.06	0.65	3.11E-04	9.35E-04
Analytical T Case 3	-2.45	0.80	3.49E-02	1.90E-01

423



424

425 Figure 7. Probability density and mass functions of hydraulic conductivity fields. Note here that

426 T is transmissivity and K is hydraulic conductivity. Note in this figure K Case G1 Top and K

427 Case G1 Bottom are from the same case and represent the Top Geology and Bottom Geology
428 portions of Figure 2. Same is true here for K Case G3 Top and K Case G3 Bottom.

429 *Hydrological Modeling Results*

430 We make use of the UCRB ParFlow-CLM results to assess the performance of our hydraulic
431 conductivity products in application. The results at all ten USGS stream gages for each of our ten
432 simulations can be found in the supporting information, Figures S9-S18. As shown in Table 3,
433 five simulations were run without any vertical flow barrier having an effective thickness
434 (combined thickness of model elements hydraulically connected to streams without a retarding
435 barrier) equivalent to the full model thickness of 1,192m. We find that our models overpredict
436 baseflow in each of these simulations (Figure 8). Regardless of overprediction, the *literature and*
437 *this study's analytical approaches* perform similarly to each other, both predicting just over
438 twice the observed values having average relative biases across all ten stream gages of 110% and
439 106% respectively. These values are slightly higher than the 75% seen in the *Case G1* modeling
440 and the 58% seen in *Case G2* but considerably less than the 652% relative bias from the *Case G3*
441 simulation. Accuracy in timing appears to be muted in all cases by the vast overprediction of
442 baseflow. Still, the two analytical approaches perform similarly with an average Spearman's Rho
443 of 0.35 for both cases. The timing in *Case G1* is marginally worse with a Spearman's Rho of
444 0.34, *Case G3* performs worst with a Rho of 0.20, and *Case G2* performs best with a Rho of
445 0.44.

446 Our results support the idea that aquifer hydraulic conductivity is an important control on
447 stream baseflow. We see cases with higher hydraulic conductivity values appear to display
448 greater overprediction. This result is clear when comparing the hydrographs of our K *Case G1*
449 simulation, which had the lowest basin-wide average K with our K *Case G3* simulation, which
450 had the highest basin-wide average K. Here, *Case G1* overpredicts 10th-percentile flows by 230%
451 on average across all ten stream gages, and *Case G3* overpredicts 10th-percentile flows by

452 1,520%. The *G2 Case* presents an anomaly in that its K values are not lower than *Case G1*, yet it
453 predicts lower baseflows. This suggests that the spatial distribution of K along with the large-
454 scale average has impacts on streamflows.

455 The impact of effective model thickness on streamflow is illustrated when a vertical flow
456 barrier is imposed on the model at specified depths. With the spatially variable vertical flow
457 barrier at an estimated depth to bedrock, we see a dramatic decrease in simulated baseflow
458 (Figure 9). However, it appears that the variable-depth vertical flow barrier has caused a
459 systematic underprediction in streamflow for both *Case G1* with a relative bias of -30% at Lee’s
460 Ferry and *Analytical K Case A7* with a relative bias of -77% at Lee’s Ferry. Our headwaters
461 perform better with the vertical flow barrier, however. This is reflected in an arithmetic mean
462 relative bias across all gages of -58% for the *Analytical K Case A7* Approach and 3% for *Case*
463 *G1*. Additionally, we see an improvement of timing, as the Spearman’s Rho for our *Analytical K*
464 *Case A7* Approach increases from 0.35 to 0.53, and *Case G1* improves from 0.34 to 0.49.

465 By comparing simulated groundwater depths with nearly 2,000 annually averaged
466 monitoring well observations, comparisons between observed and predicted WTD result in
467 RSME values ranging from 8.9m to 12.5m across ten simulations. As in our surface water
468 comparisons, the *Literature Analytical Approach* and the *Study Analytical Approach* compare
469 similarly with RMSEs of 9.25m and 9.24m respectively. Our two analytical approaches
470 outperform K *Case G1* and K *Case G3* in terms of R and R^2 , but the *Geological K Case 2* map
471 performs best overall. Correlation plots are shown in Figure 10 (without vertical flow barrier)
472 and Figure 11 (with vertical flow barrier). The similarity in performance between Analytical
473 cases 1 and 7 and the *Geological K Case 2* K field can be seen in their correlation coefficients

474 and respective plots. We associate this similarity in performance with the similarity in area-
475 weighted mean K seen between these three products.

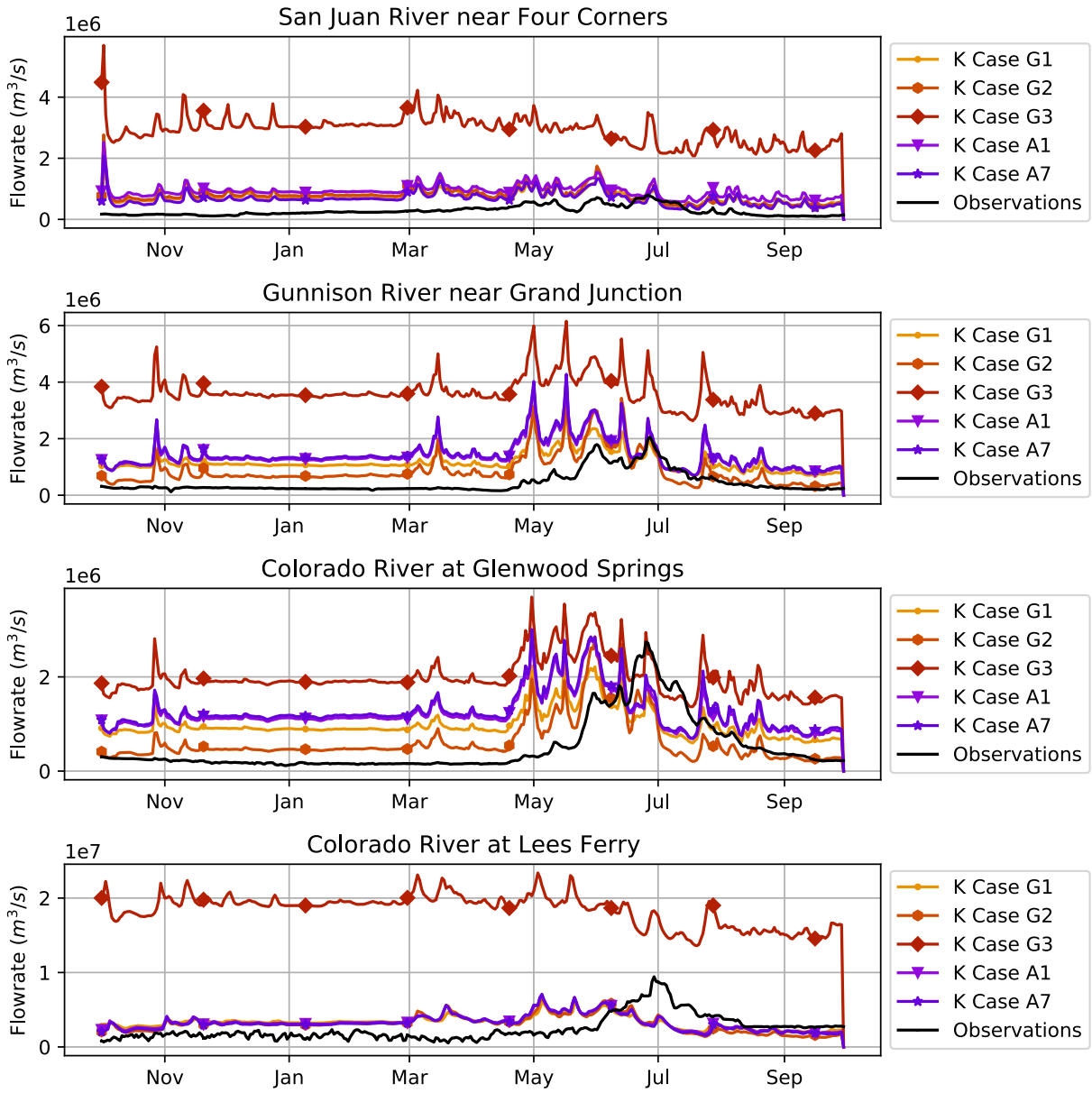
476 We find that all cases and approaches underpredict groundwater depth, meaning that the
477 elevation of the simulated water table is too high. This can be seen in Table 5, where the mean
478 deviation between observed groundwater depths and simulated groundwater depths is positive
479 for all cases. Our addition of vertical flow barriers improves this bias but hurts groundwater
480 depth predictions holistically (Figure 11). It can be seen, however, that the improvement of
481 streamflow estimates due to the vertical flow barrier is larger than the worsening of the waters
482 table depth. Maps of predicted and observed WTD can be found for all ten simulations in the
483 Supporting Information, Figures S20-S29. These K fields present the errors in observed-
484 predicted WTD and can be used to further demonstrate the spatial distribution of this error.

485

486 Table 5. Groundwater depth prediction performance statistics. Note: CFBZ indicates a constant-
 487 depth flow barrier and SFBZ indicates a variable-depth flow barrier at Shangguan’s depth to
 488 bedrock. The modified variable-depth flow barrier (mSFBZ) is located at a depth of 100m or
 489 Shangguan’s estimate of depth to bedrock, whichever is greater.

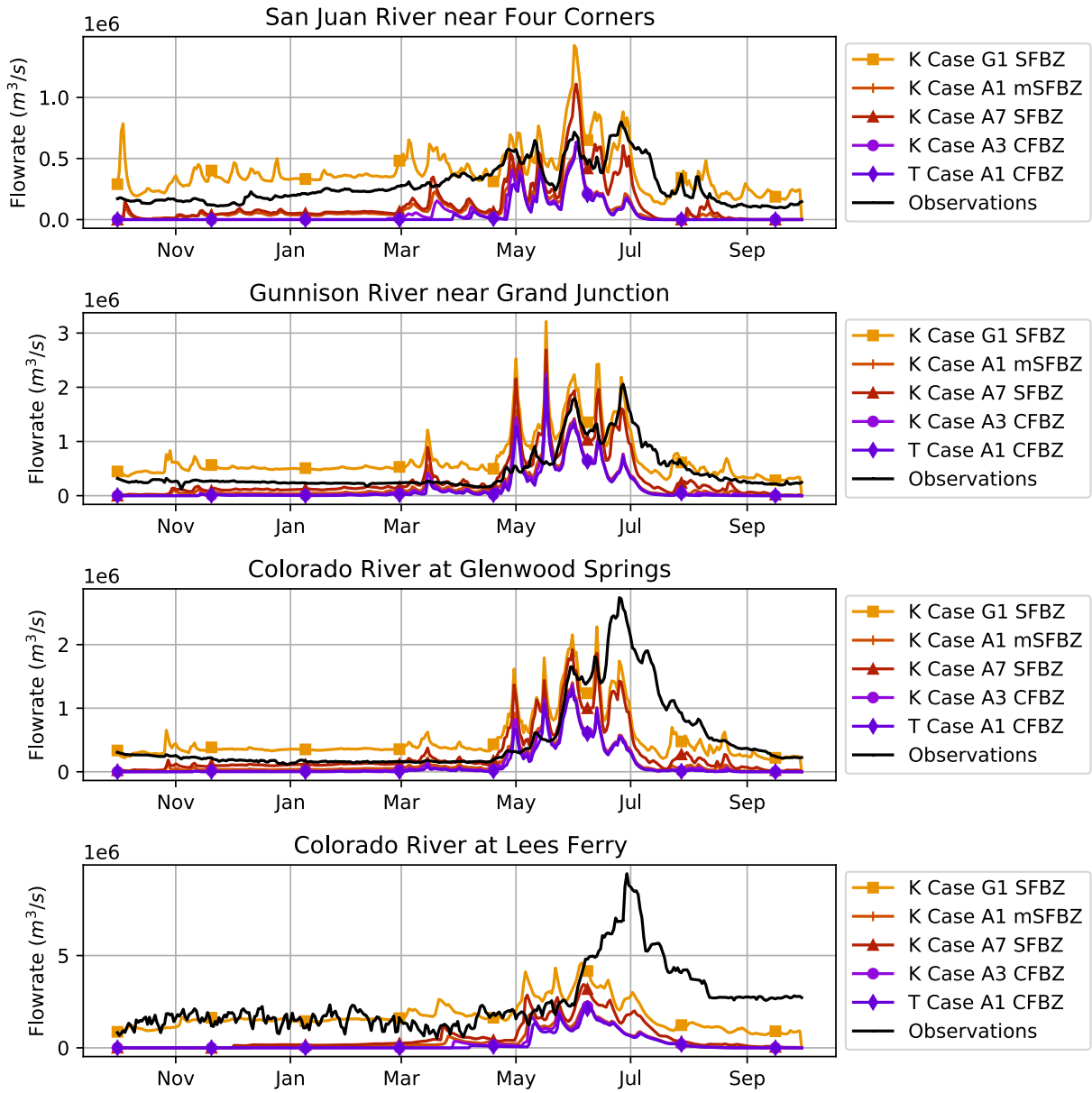
Subsurface	R²	RMSE (m)	Mean Deviation: Obs-Calc (m)
Geological K Case 1	0.40	12.5	0.24
Geological K Case 2	0.70	8.9	1.68
Geological K Case 3	0.67	9.9	1.90
Analytical K Case 1	0.68	9.3	1.52
Analytical K Case 7	0.68	9.2	1.62
Geological K Case 1 (SFBZ)	0.41	12.3	0.28
Analytical K Case 1 (mSFBZ)	0.59	10.1	0.46
Analytical K Case 7 (SFBZ)	0.62	9.8	1.55
Analytical K Case 3 (CFBZ)	0.60	10.2	0.43
Analytical T case 1 (CFBZ)	0.58	10.4	0.37

490



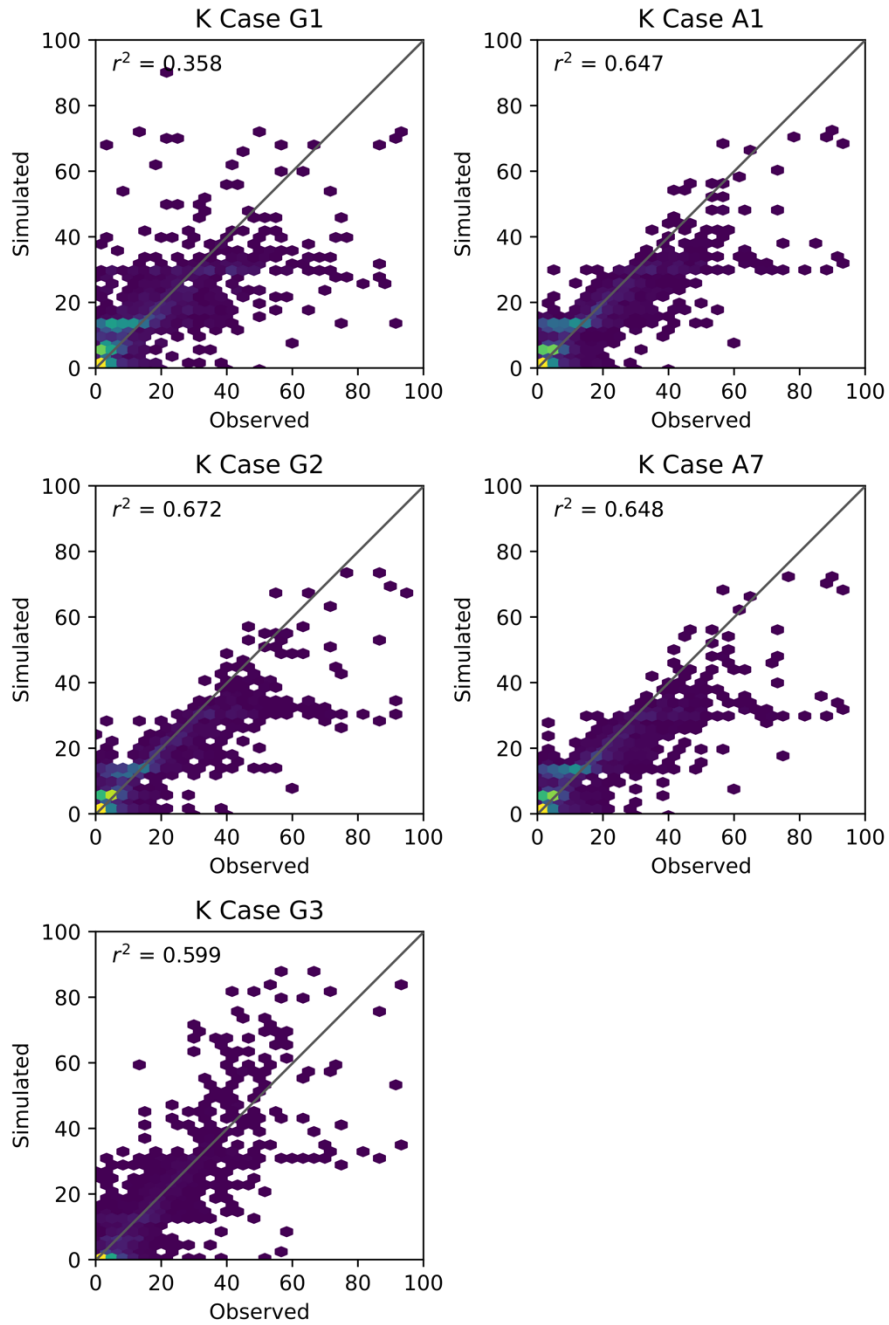
491

492 Figure 8. Hydrograph results at four representative stream gages in the UCRB.



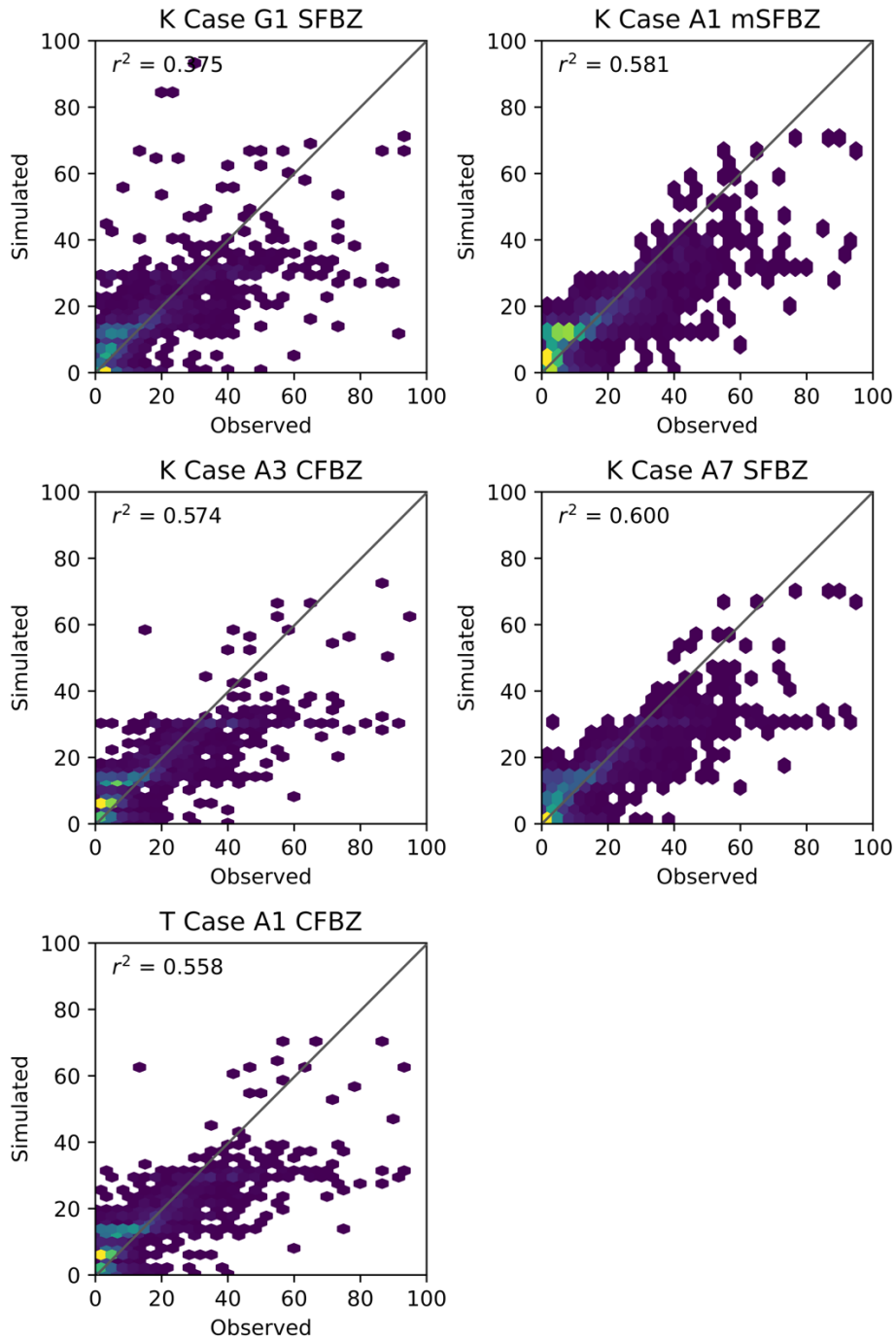
493

494 Figure 9. Hydrograph results for four selected stream gages.



495

496 Figure 10. Density scatterplots of simulated groundwater depth and observed groundwater depth
497 from Fan (Fan et al. 2013) in the UCRB for simulations without a vertical flow barrier. Note that
498 colors represent the density of points that fall within a range of values, brighter colors signify
499 that many points fall along the same location.



500

501 Figure 11. Density scatterplots of simulated groundwater depth and observed groundwater depth

502 from Fan (Fan et al. 2013) in the UCRB for simulations that include a vertical flow barrier. Note

503 that colors represent the density of points that fall within a range of values, brighter colors

504 signify that many points fall along the same location.

505 **Discussion**

506 We find analytical hydraulic conductivity fields to be smoother than geologically informed ones.
507 In the *Geological* cases the effective K values was not distributed within indicator categories as
508 there is not much information on this at large scale. Some work suggests that distributions in K
509 around effective values are important at smaller scales and finer resolution and that runoff
510 processes may average up at the hillslope scale (Meyerhoff and Maxwell, 2011). The Analytical
511 Cases distribute K values throughout as each value is determined via the analytical
512 approximation at the resolution applied, one of the reasons for conducting this comparison. This
513 finding is consistent with groundwater finding preferential flow paths around or through geologic
514 features with low hydraulic conductivity, such that even areas mapped with predominantly low K
515 geologies would have a resulting higher effective K. The same could be seen in areas that have
516 primarily high K, but poor connectivity due to low K in a few areas to bottleneck flow; although,
517 this is less common. Higher hydraulic conductivities at larger scales have been noted in literature
518 and are generally accepted as a naturally occurring phenomenon (Schulze-Makuch et al. 1999;
519 Neuman 1994). Smoother transitions in K also arise from averaging the data over HUC12
520 regions and limitations in the input datasets. For example, analytical approaches are sensitive to
521 stream density, which is limited by the scale at which it was mapped.

522 Our experiments with the vertical flow barrier suggest that the thickness of model units
523 hydraulically connected to streams plays a large role on governing baseflow. This in turn
524 suggests that these higher Ks would perform best in a hydrologic model with a shallower
525 subsurface, or one with a model feature to limit baseflow like a vertical barrier. The results from
526 our implementation of the *Literature Analytical Approach*, we see the influence of input
527 parameters on resulting K values. For example, in *Analytical K Cases 2 and 5*, we see the

528 sensitivity of the approach to valley depth (d). In these cases, valley depth was assumed to be
529 less than or equal to depth to bedrock (H). This assumption forced shallower valley depths than
530 calculated by the black-top-hat transform in areas with steep topography and shallow depths to
531 bedrock. We made this assumption to increase the number of catchments in which we could
532 analytically calculate K (in cases where valley depth is greater than twice the bedrock depth this
533 approach results in negative values of K , which are obviously non-physical). In *Literature*
534 *Analytical Cases* 1,3,4, and 6, we left valley depth unchanged and made assumptions regarding
535 bedrock depth. We see closer agreement in these cases highlighting the influence of the black-
536 top-hat transform result on K . This transform was readily performed by existing python libraries,
537 which make it easy to do, but choosing the parameters for the transform is less intuitive. The
538 black-top-hat transform requires the mapper to specify a search window shape and radius, which
539 is a difficult to infer from physical parameters.

540 The *Study Analytical Approach*, like the *Literature Analytical Approach*, is sensitive to
541 input parameters as is illustrated in the cases with model slopes and flow lengths: *Analytical K*
542 *Case 9* and *T Case 3*. The mathematical reason for these outliers is that we have effectively
543 flattened the slope and increase the flow lengths in nearly all catchments. In application, the two
544 analytical approaches explored were both doable with readily available Python tools.

545 Topographic slope to infer hydraulic gradient may or may not be a more accurate proxy for
546 hydraulic gradient but requires no parameter such as the black-top-hat's window size and
547 conceptually seems to perform better in steeply contoured mountainous aquifers.

548 Of course, this study has limitations. The hydrologic model we used should be
549 considered an example application case and not a perfect assessment of the physical truth. The
550 total transmissivity of model units interacting with streams is shown to have a large impact on

551 streamflow. We show that high K leads to higher streamflow and lower water table depths. We
552 hypothesize that this is the result of more lateral groundwater flow to streams, and less water lost
553 to evapotranspiration (ET). While water table depth is clearly linked to ET (e.g. Kollet and
554 Maxwell 2008) K-ET relationships have mostly been demonstrated at much smaller scales (e.g.
555 Atchely and Maxwell, 2011). The high streamflow values of the *K Case G3* simulation and the
556 lower, more accurate, streamflows of the cases with flow barriers are supportive of this. When
557 looking at groundwater levels in comparison to observations, we see shallower predicted water
558 tables over the majority of the domain. This systematic error could be a result of model physics,
559 as it is constant across high and low values of K. We hypothesize that the 1km resolution of our
560 model may not fully capture the steep topography of the domain, resulting in lower simulated
561 hydraulic gradients and consequently higher water tables. It is also possible that the positive
562 errors covary with the location of the wells. This is possible if wells are preferentially drilled in
563 specific areas with a physical reason to bias one way or another in our model. Consider that the
564 majority of wells may likely be drilled in lowland areas where groundwater is most accessible
565 and contributes to streamflow where streambeds have incised down to the water table. Our
566 model simulates streams without incision, so it is likely that we see a slight shallow bias for
567 water table depth in lowland areas. A challenge in this work is that there is not a clear “winner”
568 among the cases. Some cases have better streamflow, some better WTD and some of the cases
569 are better for streamflow. For example, *Case G1 SFBZ* matches the flows the best but has poorer
570 groundwater performance when compared to *Case A7 SFBZ*. These examples highlight the
571 challenges of determining a single best subsurface over a continental scale basin.

572

573 **Conclusions**

574 This study addressed the challenge of characterizing hydraulic conductivity at the continental
575 scale comparing both analytical and geologically informed approaches. We used an analytical
576 approach from literature as well as novel approach derived in this study to produce nine
577 hydraulic conductivity maps and three transmissivity maps for the contiguous United States and
578 adjacent hydrologic regions. We compared the results of analytical approaches to each other and
579 to hydraulic conductivity values from literature finding them to be similar in mean value,
580 standard deviation, and in some instances, spatial trend. We tested K data products from both
581 analytical approaches and three geology-informed approaches in a fully integrated hydrologic
582 model of a basin-scale watershed — something unique to this study.

583 We found that the hydraulic conductivity of the subsurface plays a role in surface water
584 partitioning, which highlights the interconnectedness of groundwater, soil moisture, and surface
585 water. Specifically, we saw higher mean K values produce more simulated streamflow causing
586 higher relative bias in the form of over-prediction, a result similar to prior studies conducted at
587 smaller scales (Foster and Maxwell 2019). This supports holistic approaches to conceptualizing
588 and modeling hydrology. We found that limiting the thickness and consequently the effective
589 transmissivity of simulated aquifer units by use of a vertical flow barrier has important impacts
590 for surface water as well, primarily in the form of reducing baseflow, which is groundwater
591 driven. Conversely, we found that peak flows, which were snowmelt dominated and largely
592 runoff driven in our domain, are affected less by model subsurface configuration.

593 The findings of this study support the use of geomorphology and analytical approaches to
594 make inferences about subsurface hydrostratigraphy. We found that analytical approaches yield
595 estimates of K that produce similar streamflow and WTD statistics compared to non-analytical,

596 geology-informed estimates from literature. We also show that the analytical approach derived
597 by this study, referred to herein as the *Study Analytical Approach*, produces estimates of K that
598 are similar in spatial distribution, standard deviation, mean value, and modeling performance to
599 estimates from the *Literature Analytical Approach* (Luo et al. 2010b). Moreover, the *Study*
600 *Analytical Approach* required fewer assumptions in application.

601 Finally, we conclude that the underlying assumptions of our analytical approaches, while
602 imperfect, may be useful for conceptualizing and modeling the subsurface at large scales. For
603 example, we do not capture the three-dimensional heterogeneity of hydraulic conductivity, nor
604 do we capture anisotropy. However, our approach offers utility as it has been successfully used
605 to estimate effective hydraulic conductivity at large scales.

606

607 **Acknowledgements**

608 This research has been supported by the U.S. Department of Energy Office of Science (grant no.
609 DE-AC02-05CH11231) and the US National Science Foundation Office of Advanced
610 Cyberinfrastructure (grant no. OAC- 2054506 and OAC-1835855). Data products will be made
611 available via the HydroFrame project (<https://hydroframe.org>) upon final publication. The
612 authors declare no conflict of interest. We thank the Editor in Chief (L. Konikow), Executive
613 Editor (M. Hill), and three anonymous reviewers for their constructive comments which have
614 added to the quality and clarity of this work.

615

616 **Supporting Information**

617 This article includes a Supporting Information document which contains additional figures that
618 supplement the manuscript. The Supporting Information is not peer-reviewed.

619

620

621 **References**

- 622 Ashby, S., and R. Falgout. 1996. A Parallel Multigrid Preconditioned Conjugate Gradient
623 Algorithm for Groundwater Flow Simulations. *Nuclear Science and Engineering* 124, no. 1:
624 145–159, <https://doi.org/10.13182/NSE96-A24230>.
- 625 Atchley, A.L., R.M. Maxwell. 2011 Influences of subsurface heterogeneity and vegetation cover
626 on soil moisture, surface temperature and evapotranspiration at hillslope scales. *Hydrogeol*
627 *J* 19, 289–305, <https://doi.org/10.1007/s10040-010-0690-1>
- 628 Barthel, R. 2014. A call for more fundamental science in regional hydrogeology. *Hydrogeology*
629 *Journal* 22, no. 3: 507–10, <https://doi.org/10.1007/s10040-014-1101-9>.
- 630 Belitz, K., E. Watson, T. D. Johnson, and J. Sharpe. 2019. Secondary Hydrogeologic Regions of
631 the Conterminous United States. *Groundwater* 57, no. 3: 367–377,
632 <https://doi.org/10.1111/gwat.12806>.
- 633 Bierkens, M. F. P., V. A. Bell, P. Burek, N. Chaney, L. E. Condon, C. H. David, A. de Roo, et al.
634 2015. Hyper-resolution global hydrological modelling: what is next? *Hydrological*
635 *Processes* 29, no. 2: 310–320, <https://doi.org/https://doi.org/10.1002/hyp.10391>.
- 636 Condon, L. E., and R. M. Maxwell. 2014. Feedbacks between managed irrigation and water
637 availability: Diagnosing temporal and spatial patterns using an integrated hydrologic model.
638 *Water Resources Research*, 5375–5377, <https://doi.org/10.1002/2013WR014979>.Reply.
- 639 Condon, L. E., S. Kollet, M. F. P. Bierkens, G. E. Fogg, R. M. Maxwell, M. C. Hill, H.-J. H.
640 Fransen, et al. 2021. Global Groundwater Modeling and Monitoring: Opportunities and
641 Challenges. *Water Resources Research* 57, no. 12: e2020WR029500,
642 <https://doi.org/https://doi.org/10.1029/2020WR029500>.

- 643 Condon, L. E., and R. M. Maxwell. 2013. Implementation of a linear optimization water
644 allocation algorithm into a fully integrated physical hydrology model. *Advances in Water*
645 *Resources* 60: 135–147, <https://doi.org/10.1016/j.advwatres.2013.07.012>.
- 646 de Graaf, I., L. Condon, and R. Maxwell. 2020. Hyper-Resolution Continental-Scale 3-D Aquifer
647 Parameterization for Groundwater Modeling. *Water Resources Research* 56, no. 5:
648 e2019WR026004, [https://doi.org/https://doi.org/10.1029/2019WR026004](https://doi.org/10.1029/2019WR026004).
- 649 Desbarats, A. J., C. E. Logan, M. J. Hinton, and D. R. Sharpe. 2002. On the kriging of water
650 table elevations using collateral information from a digital elevation model. *Journal of*
651 *Hydrology* 255, nos. 1–4: 25–38, [https://doi.org/10.1016/S0022-1694\(01\)00504-2](https://doi.org/10.1016/S0022-1694(01)00504-2).
- 652 Eagleson, P. S. 1986. The Emergence of Global-Scale Hydrology. *Water Resources Research*.
653 Vol. 22.
- 654 Enemark, T., L. J. M. Peeters, D. Mallants, and O. Batelaan. 2019. Hydrogeological conceptual
655 model building and testing: A review. *Journal of Hydrology* 569: 310–329,
656 [https://doi.org/https://doi.org/10.1016/j.jhydrol.2018.12.007](https://doi.org/10.1016/j.jhydrol.2018.12.007).
- 657 Enemark, T., L. Peeters, D. Mallants, B. Flinchum, and O. Batelaan. 2020. A Systematic
658 Approach to Hydrogeological Conceptual Model Testing, Combining Remote Sensing and
659 Geophysical Data. *Water Resources Research* 56, no. 8: e2020WR027578,
660 [https://doi.org/https://doi.org/10.1029/2020WR027578](https://doi.org/10.1029/2020WR027578).
- 661 Fan, Y., H. Li, and G. Miguez-Macho. 2013. Global Patterns of Groundwater Table Depth.
662 *Science* 339, no. 6122: 940–943, <https://doi.org/10.1126/science.1229881>.
- 663 Forrester, M. M., and R. M. Maxwell. 2020. Impact of lateral groundwater flow and subsurface
664 lower boundary conditions on atmospheric boundary layer development over complex

- 665 terrain. *Journal of Hydrometeorology* 21, no. 6: 1133–1160, <https://doi.org/10.1175/JHM->
666 [D-19-0029.1](https://doi.org/10.1175/JHM-D-19-0029.1).
- 667 Freeze, R. A., and J. A. Cherry. *Groundwater*. Englewood Cliffs, N.J: Prentice-Hall, 1979.
- 668 Gleeson, T., Smith, L., Moosdorf, N., Hartmann, J., Dürr, H. H., Manning, A. H., van Beek, L. P.
669 H., and Jellinek, A. M. 2011, Mapping permeability over the surface of the Earth, *Geophys.*
670 *Res. Lett.*, 38, L02401, doi:10.1029/2010GL045565.
- 671 Gleeson, T, T. Wagener, P. Döll, S. C. Zipper, C. West, Y. Wada, R. Taylor, et al. 2021. GMD
672 perspective: The quest to improve the evaluation of groundwater representation in
673 continental- to global-scale models. *Geoscientific Model Development* 14, no. 12: 7545–
674 7571, <https://doi.org/10.5194/gmd-14-7545-2021>.
- 675 Gleeson, T., N. Moosdorf, J. Hartmann, and L. P. H. van Beek. 2014. A glimpse beneath earth’s
676 surface: GLobal HYdrogeology MaPS (GLHYMPS) of permeability and porosity.
677 *Geophysical Research Letters*, 3891–3898, <https://doi.org/10.1002/2014GL059856>.
- 678 Haitjema, H. M., and S. Mitchell-Bruker. 2005. Are water tables a subdued replica of the
679 topography? *Ground Water* 43, no. 6: 781–786, <https://doi.org/10.1111/j.1745->
680 [6584.2005.00090.x](https://doi.org/10.1111/j.1745-6584.2005.00090.x).
- 681 Heath, R. 1983. Basic Ground-Water Hydrology. *U.S. Geological Survey Water-Supply Paper*.
682 2220, <https://pubs.usgs.gov/wsp/2220/report.pdf>.
- 683 Hill, M. C., and C. R. Tiedeman. 2007. *Effective Groundwater Model Calibration: With Analysis*
684 *of Data, Sensitivities, Predictions, and Uncertainty*. Wiley.
- 685 Hornberger, G., P. Wiberg, J. Raffensperger, and P. D’Odorico. 1998. *Elements of Physical*
686 *Hydrology*. Johns Hopkins University Press.

- 687 Huscroft, J., T. Gleeson, J. Hartmann, and J. Börker. 2018a. Compiling and Mapping Global
688 Permeability of the Unconsolidated and Consolidated Earth: GLobal HYdrogeology MaPS
689 2.0 (GLHYMPS 2.0). *Geophysical Research Letters* 45, no. 4: 1897–1904,
690 <https://doi.org/10.1002/2017GL075860>.
- 691 Huscroft, J., T. Gleeson, J. Hartmann, and J. Börker. 2018b. Compiling and Mapping Global
692 Permeability of the Unconsolidated and Consolidated Earth: GLobal HYdrogeology MaPS
693 2.0 (GLHYMPS 2.0). *Geophysical Research Letters* 45, no. 4: 1897–1904,
694 <https://doi.org/10.1002/2017GL075860>.
- 695 Jackson, T. J., R. Bindlish, M. H. Cosh, T. Zhao, P. J. Starks, D. D. Bosch, M. Seyfried, et al.
696 2012. Validation of soil moisture and Ocean Salinity (SMOS) soil moisture over watershed
697 networks in the U.S. *IEEE Transactions on Geoscience and Remote Sensing* 50, no. 5
698 PART 1: 1530–1543, <https://doi.org/10.1109/TGRS.2011.2168533>.
- 699 Jones, J., and C. Woodward. 2001. Newton-Krylov Methods for Variably Saturated Flow.
700 *Advances in Water Resources* 24: 763–774.
- 701 King, F. H. 1899. *Principles and conditions of the movements of ground water*. in U.S.
702 Geological Survey Nineteenth Annual Report, Part II. Washington D.C., Govt. Printing
703 Office, 39660921.
- 704 Kollet, S. J., and R. M. Maxwell. 2006. Integrated surface-groundwater flow modeling: A free-
705 surface overland flow boundary condition in a parallel groundwater flow model. *Advances*
706 *in Water Resources* 29, no. 7: 945–958, <https://doi.org/10.1016/j.advwatres.2005.08.006>.
- 707 Kollet, S. J., and R.M. Maxwell. 2008. Capturing the influence of groundwater dynamics on land
708 surface processes using an integrated, distributed watershed model, *Water Resour. Res.*, 44,
709 W02402, doi:10.1029/2007WR006004..

- 710 Luo, W., B. P. Grudzinski, and D. Pederson. 2010a. Estimating hydraulic conductivity from
711 drainage patterns—a case study in the Oregon Cascades. *Geology* 38, no. 4: 335–338,
712 <https://doi.org/10.1130/G30816.1>.
- 713 Luo, W., B. P. Grudzinski, and D. Pederson. 2010b. Estimating hydraulic conductivity from
714 drainage patterns—a case study in the Oregon Cascades. *Geology* 38, no. 4: 335–338,
715 <https://doi.org/10.1130/G30816.1>.
- 716 Luo, W., and D. T. Pederson. 2012. Hydraulic conductivity of the High Plains Aquifer re-
717 evaluated using surface drainage patterns. *Geophysical Research Letters* 39, no. 2: 1–6,
718 <https://doi.org/10.1029/2011GL050200>.
- 719 Foster, L., and R. M. Maxwell. 2019. Sensitivity analysis of hydraulic conductivity and
720 Manning’s n parameters lead to new method to scale effective hydraulic conductivity across
721 model resolutions. *Hydrological Processes* 33, no. 3: 332–349,
722 <https://doi.org/https://doi.org/10.1002/hyp.13327>.
- 723 Marshall, S. K., P. G. Cook, C. T. Simmons, L. F. Konikow, and S. Dogramaci. 2022. An
724 Approach to Include Hydrogeologic Barriers With Unknown Geometric Properties in
725 Groundwater Model Inversions. *Water Resources Research* 58, no. 7: e2021WR031458,
726 <https://doi.org/https://doi.org/10.1029/2021WR031458>.
- 727 Maxwell, R. M., L. E. Condon, and S. J. Kollet. 2015. A high-resolution simulation of
728 groundwater and surface water over most of the continental US with the integrated
729 hydrologic model ParFlow v3. *Geoscientific Model Development* 8, no. 3: 923–937,
730 <https://doi.org/10.5194/gmd-8-923-2015>.

- 731 Maxwell, R. M. 2013. A terrain-following grid transform and preconditioner for parallel, large-
732 scale, integrated hydrologic modeling. *Advances in Water Resources* 53, March: 109–117,
733 <https://doi.org/10.1016/j.advwatres.2012.10.001>.
- 734 Maxwell, R. M., and L. E. Condon. 2016. Connections between groundwater flow and
735 transpiration partitioning. *Science* 353, no. 6297: 377–380,
736 <https://doi.org/10.1126/science.aaf7891>.
- 737 Maxwell, R. M., and N. L. Miller. 2005. On the development of a coupled land surface and
738 groundwater model. *Developments in Water Science* 55, no. PART 2: 1503–10,
739 [https://doi.org/10.1016/S0167-5648\(04\)80161-8](https://doi.org/10.1016/S0167-5648(04)80161-8).
- 740 Meyerhoff, S., and R. M. Maxwell 2011. Quantifying the effects of subsurface heterogeneity on
741 hillslope runoff using a stochastic approach. *Hydrogeology Journal* 19, no. 8: 1515-1530,
742 DOI: 10.1007/s10040-011-0753-y
- 743 Neuman, S. P. 1994. Generalized scaling of permeabilities: Validation and effect of support
744 scale. *Geophysical Research Letters* 21, no. 5: 349–352,
745 <https://doi.org/10.1029/94GL00308>.
- 746 O’Neill, M. M. F., D. T. Tijerina, L. E. Condon, and R. M. Maxwell. 2021. Assessment of the
747 ParFlow–CLM CONUS 1.0 integrated hydrologic model: evaluation of hyper-resolution
748 water balance components across the contiguous United States. *Geoscientific Model
749 Development* 14, no. 12: 7223–7254, <https://doi.org/10.5194/gmd-14-7223-2021>.
- 750 O’neill, P., R. Bindlish, S. Chan, J. Chaubell, E. Njoku, and T. Jackson. 2020. Soil Moisture
751 Active Passive (SMAP) Algorithm Theoretical Basis Document Level 2 & 3 Soil Moisture
752 (Passive) Data Products, <https://openlandmap.org>.

- 753 Pederson, D. T. 2001. Stream Piracy Revisited: A Groundwater-Sapping Solution. *GSA TODAY*,
754 4–10, <https://www.geosociety.org/gsatoday/archive/11/9/pdf/i1052-5173-11-9-4.pdf>.
- 755 Pedregosa, F. G. Varoquaux, A. Gramfort, V. Michel, B. Thirion, O. Grisel, M. Blondel, P.
756 Prettenhofer, et al.. 2011. Scikit-learn: Machine Learning in Python. *J. Mach. Learn. Res.*
757 12, (2/1/2011), 2825–2830.
- 758 Rodriguez, F., E. Maire, P. Courjault-Radé, and J. Darrozes. 2002. The Black Top Hat function
759 applied to a DEM: A tool to estimate recent incision in a mountainous watershed (Estibère
760 Watershed, Central Pyrenees). *Geophysical Research Letters* 29, no. 6: 2–5,
761 <https://doi.org/10.1029/2001GL014412>.
- 762 Scanlon, B. R., Z. Zhang, H. Save, A. Y. Sun, H. M. Schmied, L. P. H. van Beek, D. N. Wiese,
763 et al. 2018. Global models underestimate large decadal declining and rising water storage
764 trends relative to GRACE satellite data. *Proceedings of the National Academy of Sciences*
765 *of the United States of America* 115, no. 6: E1080–E1089,
766 <https://doi.org/10.1073/pnas.1704665115>.
- 767 Schulze-Makuch, D., D. A. Carlson, D. S. Cherkauer, and P. Malik. 1999. Scale Dependency of
768 Hydraulic Conductivity in Heterogeneous Media. *Ground Water* 37, no. 6: 904–919,
769 <https://doi.org/10.1111/j.1745-6584.1999.tb01190.x>.
- 770 Shangguan, W., T. Hengl, J. Mendes de Jesus, H. Yuan, and Y. Dai. 2017. Mapping the global
771 depth to bedrock for land surface modeling. *Journal of Advances in Modeling Earth*
772 *Systems* 9, no. 1: 65–88, <https://doi.org/10.1002/2016MS000686>.
- 773 Soil Survey Staff. n.d. Web Soil Survey - Natural Resources Conservation Service, United States
774 Department of Agriculture, <https://websoilsurvey.nrcs.usda.gov/>, retrieved 8/2/2020.

- 775 Tapley, B. D., S. Bettadpur, M. Watkins, and C. Reigber. 2004. The gravity recovery and climate
776 experiment: Mission overview and early results. *Geophysical Research Letters* 31, no. 9: 1–
777 4, <https://doi.org/10.1029/2004GL019920>.
- 778 Tashie, A., T. Pavelsky, L. Band, and S. Topp. 2021. Watershed-Scale Effective Hydraulic
779 Properties of the Continental United States. *Journal of Advances in Modeling Earth Systems*
780 13, no. 6, <https://doi.org/10.1029/2020MS002440>.
- 781 Tran, H., J. Zhang, J.-M. Cohard, L. Condon, and R. Maxwell. 2020. Simulating groundwater-
782 streamflow connections in the Upper Colorado River Basin. *Groundwater* 58: 392–405,
783 <https://doi.org/10.1111/gwat.13000>.
- 784 Turner, A. K. 1992 *Three-Dimensional Modeling with Geoscientific Information Systems*.
785 Springer Dordrecht, 443p, <https://doi.org/10.1007/978-94-011-2556-7>
- 786 U.S. Geological Survey. 2019. Attributes for NHDPlus Catchments (Version 1.1) for the
787 Conterminous United States: Hydrologic Landscape Regions. *Data Series*.
- 788 Velpuri, N. M., G. B. Senay, and J. T. Morisette. 2015. Evaluating New SMAP Soil Moisture for
789 Drought Monitoring in the Rangelands of the US High Plains. *Rangelands* 38, no. 4: 183–
790 190, <https://doi.org/10.1016/j.rala.2016.06.002>.
- 791 Xia, Y., C. Peter-Lidard, M. Huang, H. Wei, and M. Ek. 2014. Improved NLDAS-2 Noah-
792 simulated hydrometeorological products with an interim run. *Hydrological Processes* 29:
793 780–792, <https://doi.org/10.1002/hyp.10190>.
- 794 Zell, W. O., and W. E. Sanford. 2020. Calibrated Simulation of the Long-Term Average Surficial
795 Groundwater System and Derived Spatial Distributions of its Characteristics for the
796 Contiguous United States. *Water Resources Research* 56, no. 8: e2019WR026724,
797 <https://doi.org/https://doi.org/10.1029/2019WR026724>.

798 Zhang, J., L. E. Condon, H. Tran, and R. M. Maxwell. 2021. A national topographic dataset for
799 hydrological modeling over the contiguous United States. *Earth System Science Data* 13,
800 no. 7: 3263–3279, <https://doi.org/10.5194/essd-13-3263-2021>.

801